Article

Not peer-reviewed version

MIL-100(Fe)-Enabled Oral Delivery of Syringic Acid with Enhanced Pharmacokinetics

Joshua Hernandez Santos *, Hannah Jean Victoriano, Mary Sepulveda, Hung-En Liu, Shierrie Mae Valencia, Rikkamae Zinca Marie Walde, Emelda Asoy Ongo, Chia-Her Lin *

Posted Date: 24 July 2025

doi: 10.20944/preprints202507.1970.v1

Keywords: syringic acid; bioavailability; MIL-100(Fe); AUC; MOF

 doi:10.20944/preprints202507.1970.v1

Article

MIL-100(Fe)-Enabled Oral Delivery of Syringic Acid with Enhanced Pharmacokinetics

Joshua Santos [1,2,*], Hannah Jean Victoriano [2], Mary Sepulveda [2], Hung-En Liu [3], Shierrie Mae N. Valencia [2], Rikkamae Zinca Marie L. Walde [2], Emelda A. Ongo [1,2] and Chia-Her Lin [4]

[1] Department of Science and Technology – Central Office, General Santos Avenue, Upper Bicutan, Taguig City 1631, Philippines

[2] Department of Science and Technology – Industrial Technology Development Institute, General Santos Avenue, Upper Bicutan, Taguig City 1631, Philippines

[3] Department of Chemistry, National Taiwan Normal University, No. 162, Section 1, Heping E Rd, Da'an District, Taipei City 106 , Taiwan

[4] Department of Chemistry, National Tsing Hua University, 101, Section 2, Kuang-Fu Road, Hsinchu 300044, Taiwan

* Correspondence: jhsantos120@gmail.com; Tel.: (+632) 8837-2071 to 82 local 2276

Abstract

Background/Objectives: Plant-derived bioactive compounds like syringic acid, a phenolic acid from the shikimic acid pathway, have shown potential against chronic diseases including diabetes, cardiovascular disorders, cancer, and cerebral ischemia. However, its poor water solubility and rapid systemic elimination result in low bioavailability, limiting therapeutic potential. This study aimed to enhance its bioavailability using MIL-100(Fe), a metal-organic framework (MOF) known for high surface area and drug-loading capacity. **Methods:** MIL-100(Fe) was synthesized using an optimized method and loaded with syringic acid through impregnation at 12, 24, 36, and 48 hours. Characterization included PXRD, FTIR, BET, SEM, and DLS. Acute oral toxicity was evaluated following OECD 425 guidelines, and bioavailability was assessed in Sprague Dawley rats. **Results:** The 1:2 syringic acid to MIL-100(Fe) ratio achieved the highest drug loading at 64.42 ± 0.03% (12 h). PXRD and FTIR confirmed successful loading (notably at 1242 cm^{-1}), and TGA indicated thermal stability at ~450 °C. SEM revealed octahedral particles with an average size of 270.67 ± 2.60 nm. BET showed reduced surface area post-loading. In vitro drug release exhibited media-dependent profiles. Toxicity tests indicated no adverse effects at 2000 mg/kg. Oral administration of SYA@MIL-100(Fe) resulted in a 10.997-fold increase in relative bioavailability versus oral syringic acid and 12.82-fold over intraperitoneal administration. **Conclusions:** MIL-100(Fe) is a safe and effective oral carrier for syringic acid, significantly enhancing its bioavailability. This platform shows strong potential for delivering phenolic compounds in pharmaceutical applications.

Keywords: syringic acid; bioavailability; MIL-100(Fe); AUC; MOF

1. Introduction

Natural compounds can also serve as parent molecules or leads that can be optimized and synthesized into better compounds. Around 60% of the commercial products are derived from natural sources. The recent approaches in drug discovery revitalize the interest in natural products in combating other diseases and multi-resistant infections [1]. Despite the numerous pharmacological activities of these compounds, their use is limited due to their low bioavailability. Such limitation can be due to the physicochemical properties of the compounds and the disposition in the gastrointestinal tract. In particular, some of the causes of low bioavailability include solubility, chemical stability,

 doi:10.20944/preprints202507.1970.v1

plasma stability, gut microflora transformation, permeation and transport mechanisms, and metabolism [2].

Phenolic acids derived from plants are exhibiting good antioxidant activity, which can be correlated to the prevention or treatment of oxidative stress-induced diseases such as malignancy, diabetes, liver disease, and cardiovascular diseases [3,4]. In some studies, they can prevent neurodegenerative diseases like Alzheimer's Disease [5]. Some compounds exhibit both antioxidant and antimicrobial activities as well [6]. This group of secondary metabolites is derived from the biosynthesis of L-phenylalanine or L-tyrosine. Their structure is noted to have one or more hydroxyl groups attached to the aromatic ring [7,8]. In particular, phenolic or phenolcarboxylic acid is characterized as possessing at least one carboxylic acid moiety. They are diversely located in different plant parts and are usually found in the carboxylic acid derivative form, such as amides, esters, or glycosides [9].

Syringic acid (as illustrated in Figure 1-1) is a diversely distributed phenolic compound found in olives, dates, spices, squash, grapes, acai palm, honey, red wine, and many other plants [10,11]. This phenolic compound has prevented or inhibited oxidative stress, microbial growth and infection, inflammation, cancer/malignancy, and diabetes mellitus. Protection in major organs has been noted in the heart, liver, and brain [4]. Due to its poor solubility and fast elimination in the body, the bioavailability of syringic acid was noted to be low [12]. Good evidence of the fast elimination of syringic acid is the absolute bioavailability of syringic acid when administered intravenously to the ear of rabbits, accounting for 86.27% instead of the 100% absolute bioavailability [13]. Other formulation studies for syringic acid have resulted in a higher area under the curve (120.58 ± 2.92 and 338.08 ± 3.65 g min/ mL for pristine syringic acid and SA-liposome, respectively) but still having the same Cmax and Tmax (4.50 ± 0.04 g/mL, and 8 minutes, respectively) [12].

Numerous approaches have been reported in enhancing the bioavailability of natural products, such as physical and chemical modifications of the compound, particle size reduction, crystal engineering, salt formation, solid dispersion, use of surfactants, complexation, and so forth [14]. The use of drug delivery systems enables the effective transport of drugs into the systemic circulation by modifying the drug release profile, capacity to permeate biological barriers, and affects biodistribution and pharmacokinetics [15]. Although many delivery systems have been formulated, there are still some limitations to each delivery system. Therefore, newer materials and methods need to be tested to overcome these limitations. One promising avenue to address this is the use of inorganic and metallic precursors for the preparation of a new drug delivery system, which marks the transition from conventional polymers. Highly porous inorganic materials are considered candidates for the delivery of different drugs, carrying the advantages in preparation and formulation, such as encapsulation, controlled release, and improved organ targeting [16].

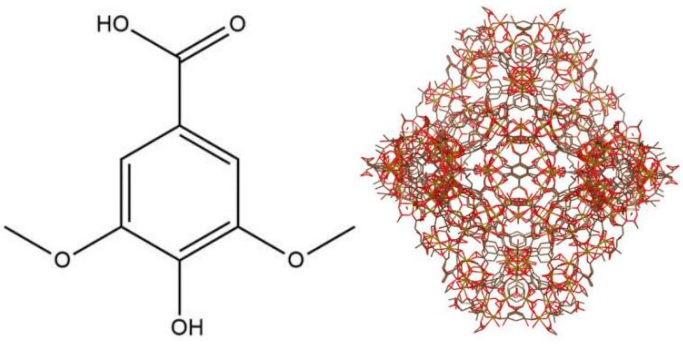

1 2

Figure 1. The structure of the (1) phenolic acid, syringic acid, 3,5-Dimethoxy-4-hydroxybenzoic acid, and (2) MIL-100(Fe) (as visualized using VESTA, version 2025, Japan).

 doi:10.20944/preprints202507.1970.v1

Among these highly porous materials are metal-organic frameworks (MOFs). These are novel polymers made of metal ions or may come in metal clusters that form multidentate organic porous ligands [17]. They are widely used in biological sensing, catalysis, and gas storage due to the following characteristics: (1) high surface area; (2) tunable pore size; (3) three-dimensional rigid skeleton; (4) organic-inorganic hybrid nature; and (5) versatile crystal morphology. Different kinds of metal-organic frameworks exist such as ZIF-8(Zn), HKUST-1(Cu), Uio-66(Zr), Hf-MOF-888, Zn-MOF-3, CD-MOF-1, CD-MOF-2, Uio-66(Zr)-NO2, MIL-53(Fe), MIL-88(Fe), and MIL-100(Fe) [18]. Some of the drugs formulated with the metal-organic framework as a drug delivery system include ibuprofen, azidothymidine, cidofovir, gemcitabine, topotecan, isoniazid, doxycycline, tetracycline, docetaxel, lamivudine, cidofovir, exthoxysuccinatocisplatin, oridonin, caffeine, 5-fluorouracil, mitoxantrone, etilefrine, cisplatin, ketoprofen, lansoprazole, azilsartan, budesonide, valsartan, doxorubicin, and many more [19–41]. In particular, Mil-100(Fe) (Figure 1-2) was used as the drug carrier in this study.

Therefore, this project aims to address the limited bioavailability of syringic acid. Specifically, this project aims to prepare and synthesize MIL-100(Fe), a metal-organic framework, as a drug delivery system for the natural product, syringic acid. Characterization of the prepared drug delivery system will be done based on its particle size, zeta potential, entrapment efficiency, drug loading, surface morphology, BET surface area and FT-IR. The in vitro drug release study of the drug delivery system will be determined in three release media namely, simulated gastric fluid pH 1.2, simulated intestinal fluid pH 6.8, and Phosphate buffered saline pH 7.4. The possible release mechanism of the preparation will be determined using five drug release models. The toxicity of the preparation will be tested in a non-mammalian model using cell-based toxicity and a murine model. Likewise, the bioavailability of the preparation will be determined in the rabbit model. A comparison of the Area under the curve using the pristine and incorporated syringic acid will be used as a point of comparison to whether the use of the drug delivery system has achieved its intended purpose. This project aims to enhance the bioavailability of syringic acid.

2. Materials and Methods

2.1. Materials and Reagents

Syringic acid (≥ 95%) was purchased from Sigma-Aldrich (St. Louis, MO, USA). Ferric nitrate nonahydrate ($Fe(NO_3)_3 \cdot 9H_2O$, analytical grade) and trimesic acid (benzene-1,3,5-tricarboxylic acid, ≥ 98%) were obtained from standard commercial suppliers. Iron(II) chloride tetrahydrate ($FeCl_2 \cdot 4H_2O$), sodium hydroxide (NaOH), and ethanol (95%) were purchased locally. Deionized water was prepared using a Milli-Q ultrapure water system. All reagents and solvents were used without further purification.

2.2. Animals

Male Sprague Dawley (SD) rats (200–250 g) were obtained from the Laboratory Animal Facility of the Department of Science and Technology–Industrial Technology Development Institute (DOST–ITDI, Taguig City, Philippines). All animal test procedures were done at the Laboratory Animal Facility of the Department of Science and Technology–Industrial Technology Development Institute (DOST–ITDI, Taguig City, Philippines). The animals were housed under standard laboratory conditions with a controlled temperature of 25 ± 2 °C and relative humidity of 45 ± 5%, and maintained on a 12 h light/dark cycle. Rats were given distilled water and standard laboratory chow ad libitum and were acclimatized for 7 days prior to experimentation. All animal procedures were reviewed and approved by the Institutional Animal Care and Use Committee (IACUC) of DOST–ITDI, in accordance with the guidelines set by the Bureau of Animal Industry (BAI) of the Philippines (AR-2024-0138). Prior to drug administration, animals were fasted for 12 hours with free access to distilled water. All animal test procedures were supervised by a licensed veterinarian.

 doi:10.20944/preprints202507.1970.v1

2.3. Methods

2.3.1. Synthesis of MIL-100

Synthesis of MIL-100(Fe) was done following the procedure outlined by Luo and co-workers [42]. The reaction was done by dissolving 1.14 mmol (226.64 mg) of iron (II) chloride tetrahydrate, 0.79 mmol (166.01 mg) of trimesic acid, and 2.28 mmol (91.2 mg) of sodium hydroxide in 60 mL of deionized water. The mixture was stirred at room temperature for 24 hours. The solution was centrifuged at 5000 rpm for 10 minutes to collect the MOF powder [43]. The MOF powder was washed with 60 mL of deionized water for 30 minutes at 80 °C three times, subjecting the MIL-100(Fe) powder in centrifugation at 5000 rpm for 10 minutes. The MOF powder was washed with 95% ethanol at 80°C for 30 minutes, subjecting the MIL-100(Fe) powder to centrifugation at 5000 rpm for 10 minutes. The slurry pellet mixture was dried under vacuum at 80 °C for 30 minutes (as illustrated in **Figure 2**).

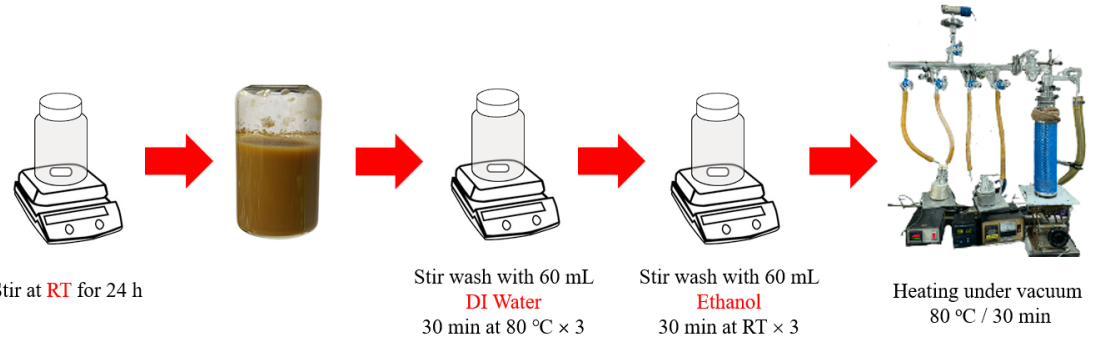

Figure 2. Schematic diagram of the MIL-100(Fe) synthesis using the method of Luo et al [42].

2.3.2. Syringic Acid Impregnation and Quantification

The syringic acid, a solid phenolic acid, was purchased from Sigma-Aldrich (> 95%). The loading of the magnolol to the MOF drug carriers was done through simple drug impregnation as reported in separate studies of Cunha and co-workers, and Singco and co-workers [21,44].

Approximately 100 mg of MIL-100(Fe) was stirred with the syringic acid ethanolic solution (1 MOF:1 SYA) (100 µL solution per 1 mg MOF). The syringic acid entrapment protocol was carried out in 4-time frames (12 hours, 24 hours, 36 hours, and 48 hours) with a stirring speed of 75 rpm. After the given period of entrapment, the mixture was centrifuged at 10,000 rpm for 10 minutes. The supernatant liquid will be separated and stored for further analysis. The MOF particle was washed with 12 mL of 95% ethanol to remove the superficially adsorbed syringic acid. The mixture was re-centrifuged at 10,000 rpm for 10 minutes to separate the particles with the supernatant liquid; the procedure of washing and centrifugation was done three times. The preparation containing syringic acid impregnated into the MIL-100(Fe) was labeled as "*SYA@MIL-100(Fe)*". The preparation was dried at 80 °C and stored for further analysis [44].

The amount of syringic acid impregnated into MIL-100(Fe) was calculated by determining the unabsorbed syringic acid found in the supernatant liquid using high performance liquid chromatography method using HPLC Shimadzu 2050C PDA model with InertSustain C18 5 µm, 150 x 4.6mm ID column (GL Science, Shinjuku-ku, Tokyo, 163-1130 Japan) equipped with Photodiode array (PDA) (Shimadzu, Japan). The detection wavelength was optimized at 272 nm with the flow rate of 1.0 mL/min using 70:30 water: methanol with 0.1% acetic acid [44,45].

$$Drug\ Loading\ Percent = \frac{TA-SA}{TA}\ x\ 100 \qquad (1)$$

Where TA – Total amount of syringic acid (mg); SA – amount of syringic acid in supernatant (mg).

2.3.3. Characterization of SYA@MIL-100(Fe)

Nitrogen Sorption Isotherms

 doi:10.20944/preprints202507.1970.v1

Samples were outgassed under high vacuum at 150 °C for 48 hours under vacuum condition using the Nitrogen adsorption-desorption equipment to remove residual solvents adhered inside the MIL-100(Fe) using the Quantachrome Nova 2200 instrument and pore size surface area analysis (Anton Paar QuantaTec Inc., Taipei, Taiwan). The Brunauer–Emmett–Teller (BET) specific surface area (SBET (m2/g)) was calculated from the linear part of the BET plot [46].

Thermogravimetric analysis

Samples (5-10 mg) of the pristine MIL-100(Fe) and SYA@MIL-100(Fe) were placed into the ceramic pans and heated from 50 to 800 °C with a heat rate of 10 °C/min under a nitrogen atmosphere (20 mL/min). Temperature vs. percent weight loss was graphed to determine the change between the pristine MIL-100(Fe) and SYA@MIL-100(Fe) [47].

Powder X-ray Diffraction (PXRD)

Samples were subjected to Powder X-ray Diffraction (PXRD) to check the identity and structure integrity of MIL-100(Fe) after exposure to syringic acid for different loading times. The PXRD patterns were determined at 30 kV and 10 mA with monochromated Cu K_ radiation and a scan speed of 0.5–3.5 s/step and a step size of 0.03. Two thetas were determined at 50 to 50° D8 Phase Bruker (Bruker, Taiwan) [48,49].

Fourier Transform Infrared Spectroscopy

Samples were scanned at 400 to 4000 cm^{-1} using potassium bromide pellets. The functional groups of the samples were compared to check the presence of syringic acid in the framework.

Scanning Electron Microscope

Samples were dried under vacuum and mounted on carbon double adhesive tape. The samples were coated with platinum under an argon atmosphere and reduced pressure to increase the conductivity of the sample. The analysis was done at 20,000 magnifications with 15,000 accelerating voltage using field emission scanning electron microscopy (JEOL JEM-700F) (JEOL, Hsinchu, Taiwan). Micropictographs were obtained for every sample [45,50].

Particle Size Determination

Samples were reconstituted with ultrapure water with a refractive index of 1.33 at 25 °C and 78,304 dielectric constants to make a 100-ppm concentration and sonicated for 10 minutes at 40 kHz to facilitate the distribution of the particles. Particle size was determined using the dynamic light scattering method (Nanopartica nanoparticle analyzer SZ-100V2) (Horiba Scientific, LTD, Japan) [45,50].

2.3.4. In Vitro Drug Release Study

Syringic acid and SYA@MIL-100(Fe) were subjected to an *in vitro* drug release study using the sample and separation method [45,51]. The release media used were ultra-pure water, 0.1 N Phosphate Buffer Saline (PBS) pH 7.4 for simulated blood pH, PBS pH 6.8 for simulated intestinal fluid, and 0.1 N HCl pH 2.0 for simulated gastric fluid. An appropriate amount of the sample (the amount of samples was more than three times of the solubility (g per mL) to reach the sink condition) was prepared for 100 mL of the release media. The setup was stirred at 75 rpm at 37.5 ± 0.5 °C. An aliquot of 1000 µL were taken at the time points of 5, 15, 30, 60, 120, 180, 240, 360, 1440, 1680, and 1800 minutes. A fresh amount of the media was used to compensate for the amount of the release media taken at every time point. The aliquots were centrifuged at 5000 rpm for 10 minutes. The supernatant liquid was stored for syringic acid quantification using HPLC analysis while the pellets were returned to the setup. The cumulative released amount of syringic acid from the MIL-100(Fe) was utilized to predict and correlate the behavior of the *in vitro* release. The experimental data were fitted to five predictable models: zero-order, first-order, Higuchi, Korsmeyer–Peppas, and Hixson–Crowell models[52]. Data fitting was performed by linear regression using Microsoft Excel. The correlation coefficient (r^2) was utilized as a criterion for selecting the best model that describes the release profile in the three media. The value of r^2 close to 1 signifies the best correlation.

2.3.5. Acute Oral Toxicity

 doi:10.20944/preprints202507.1970.v1

Acute oral toxicity was done in accordance with the Organization for Economic Cooperation and Development guidelines for testing chemical compounds using the acute toxic class method (OECD procedure 423).Prior to dosing, 1 mL of the blood was extracted from the test animals (Male Sprague Dawley Rats, 200-250 grams) using tail vein method and was submitted for alanine aminotransferase (ALT), aspartate aminotransferase (AST), and blood urea nitrogen (BUN) and creatinine level determinations for signs of liver and kidney damages, respectively. A dose of 2000 mg kg^{-1} was given to three test animals, and they were observed for one week. Since no test animals were recorded to show any signs of toxicity or death, an additional three test animals were given the same dose. The test animals were observed for 14 days post administration for signs of toxicity and death. After the 14 days of observation, the test animals were sedated using Zoletil 50 (50 mg tiletamine base, 50 mg zolazepam base, and 57.7 mg mannitol per milliliter) at a dose of 50 mg kg^{-1} prior to blood extraction using the cardiac puncture method. The animals were euthanized using a carbon dioxide chamber. The blood samples were analyzed for liver and kidney functions. The major organs, such as the liver and kidneys of the test animals, were harvested for tissue mounting and histopathological analysis.

2.3.6. Oral Bioavailability and Tissue Distribution

The bioavailability study of syringic acid and tissue distribution in the liver and kidney was done according to the method of Ding et al, Sun et al and Santos et al [45,53,54]. The test animals were grouped into 10 groups (n =3) for every time point (15-, 30-, 60-, 120-, 240-, 480-, 1080-, 1440-, 2880-, and 4320 minutes). The test animals were dosed at 100 mg kg^{-1} bodyweight of syringic acid and an equivalent amount of syringic acid in SYA@MIL-100(Fe) orally, while 25 mg kg^{-1} bodyweight of syringic acid and 3 mg kg^{-1} bodyweight of SYA@MIL-100(Fe) were administered to a fasted test animal. The reduction in the dosing for the intraperitoneal route is to prevent the abdominal distress of the test animal post administration.

Collection and processing of Blood Samples

After the given timepoints, the test animals were sedated using Zoletil 50 (50 mg tiletamine base, 50 mg zolazepam base, and 57.7 mg mannitol per milliliter) at a dose of 1 mg/kg before blood extraction using the cardiac puncture method. The blood was allowed to clot and centrifuged at 4000 rpm at 4°C for 5 minutes to obtain the serum. The sera were mixed with an equal amount of methanol to precipitate proteins and centrifuged again to obtain the deproteinized sera. The procedure was repeated until no precipitation with methanol occurred. The protein-free sera were dried under reduced pressure for prior analysis using HPLC.

Collection and processing of Organ Samples

After the blood collection from the test animals, the animals were euthanized, and the organs, such as the liver and kidneys, were taken. The organs were pat-dried and weighed to determine the amount of NSS to be used for homogenization (1mL of NSS per 700 mg of organ). The organs were homogenized and mixed with equal amounts of absolute ethanol. The mixture was centrifuged at 5000 rpm for 10 minutes. The serum samples were supplemented with an equal amount of absolute ethanol to facilitate the precipitation of proteins. This procedure was done until no precipitation occurred. The supernatant was allowed to dry under reduced pressure before HPLC analysis.

Syringic Acid Quantification

Samples were constituted using the mobile phase (70:30 water: methanol with 0.1% acetic acid) before HPLC analysis. The PDA detector was set at 218 nm using a gradient phase at a flow rate of 1 mL/min of 0-80% methanol for 10 minutes.

2.3.7. Statistical Analysis

All experiments were conducted in triplicate. Statistical analysis of significance was performed using SPSS 20 statistical software (SPSS Inc., Chicago, IL, USA). Differences within the group were evaluated using a paired sample t-test, while differences between various groups were evaluated

 doi:10.20944/preprints202507.1970.v1

using one-way analysis of variance (ANOVA), and a p-value < 0.05 indicated statistical significance. Post hoc analysis was done using Tukey HSD.

3. Results

3.1. Syringic Acid Impregnation and Quantification

Syringic acid was impregnated into MIL-100(Fe) at 12, 24, 36, and 48 hours at 1:1 (1 mg syringic acid: 1 mg MIL-100(Fe)) and 1:2 (2 mg syringic acid: 1 mg MIL-100(Fe)) ratios as illustrated in **Figure 3**. The mean drug loading was significantly highest at 12 hours loading (26.48% ± 0.03%) at a p-value of less than 0.001, following it is 36 hours (26.38% ± 0.02%), 48 hours (19.79% ± 0.02%), and 24 hours (19.28% ± 0.02%) at p values of less than 0.001. Interestingly, the mean percent drug loading of syringic acid decreased upon the constant value of the ratio, except for 12 hours, between the MIL-100(Fe) and syringic acid despite the change being significantly different (at p-value of less than 0.001), the difference was not remarkable (deviation of 1.76%). The drug loading of the 1:2 ratio resulted in the mean drug loading values of 64.42 ± 0.03% (12 hours) > 43.30 ± 0.17% (36 hours) > 39.12 ± 0.03% (24 hours) > 34.78 ± 0.04% (48 hours). In congruence with the entrapment efficiency data of the 1:2 ratio, the mean drug loading at 24 hours and 48 hours is deemed as non-significant at a p-value of 0.922. Two-way ANOVA data suggested that the loading ratio and loading time have a significant effect on the drug loading of syringic acid in MIL-100(Fe) at a p-value of less than 0.001. Likewise, the combined effects of loading ratio and loading time on the drug loading at a p-value of less than 0.001.

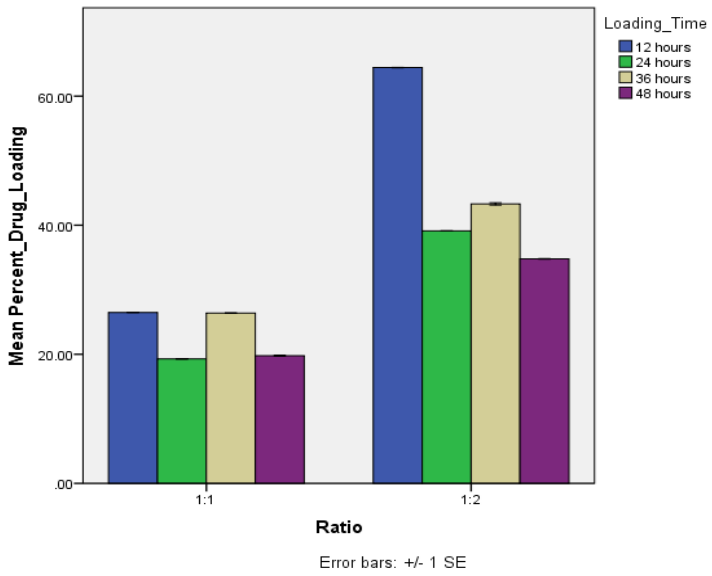

Figure 3. Mean drug loading efficiency of syringic acid at four different time point. Data presented is mean ± S.E.M.

3.2. Powder X-Ray Diffraction (PXRD)

Powder X-ray diffraction (PXRD) analysis of the synthesized MIL-100(Fe) confirmed the successful formation of the intended metal-organic framework, as shown by the characteristic peaks at 2θ values of 3.48, 4.09, 5.33, 5.49, 5.97, 6.37, 10.34, and 11.13, consistent with simulated MIL-100(Fe) patterns. These distinct Bragg peaks were conserved even after exposure to syringic acid at the different time points (12-,24-,36-, and 48-hours), indicating the structural stability and crystallinity of the MIL-100(Fe) framework despite drug loading as shown in **Figure 4A**. Furthermore, the absence of additional peaks associated with free syringic acid confirms that no recrystallized drug remained outside the pores, supporting the successful encapsulation within the MOF structure.

 doi:10.20944/preprints202507.1970.v1

3.3. Fourier Transform Infrared Spectroscopy

Fourier Transform Infrared Spectroscopy (FTIR) was used to analyze the functional groups present in the MIL-100(Fe) and SYA@MIL-100(Fe) samples. The main difference in the FTIR spectra of the two was the appearance of a peak (marked red in **Figure 4B)** in the SYA@MIL-100(Fe) samples (12- to 48-hours loading time), which corresponds to an aromatic ring attached to an ether group (C–O in Ar–O, typically found in the 1220–1260 cm^{-1} region). This functional group is absent in trimesic acid, the organic ligand used in MIL-100(Fe), but present in syringic acid. The absence of this peak in MIL-100(Fe) and its presence in SYA@MIL-100(Fe) confirm the successful impregnation of syringic acid into the metal-organic framework.

3.4. Nitrogen Adsorption-Desorption

Changes in the BET surface area of the unloaded MIL-100(Fe) and Syringic acid-loaded MIL-100(Fe), from 2028 m^2/g to 1451 m^2/g (12 hours), 1311 m^2/g (24 hours), 1274 m^2/g (36 hours), and 1007 m^2/g (48 hours) indicated the successful impregnation of syringic acid into the framework as depicted in **Figure 4C**. The reduction in the BET surface area from the pristine MIL-100(Fe) to the SYA@MIL-100(Fe) indicates the degree of mesopore content in MIL-100(Fe). A sharp increase in nitrogen adsorption at low pressure and overlapping of the adsorption-desorption isotherms in MIL-100(Fe) indicates a microporous structure. The same findings were also observed in previous studies [55–58].

3.5. Thermogravimetric Analysis

Initial weight loss observed at 100°C indicates water loss and other organic solvents that are possibly adsorbed from the environment. Degradation around 450°C indicates a high thermal stability of MIL-100(Fe). Around 300 to 400°C, small changes in the percent weight can be observed mainly due to the structural collapse of the framework. At around 450°C, a drastic decrease in the percent weight is observed due to the continuous decomposition of MIL-100(Fe) and the reduction of iron, as illustrated in **Figure 4D**.

In comparison with the unloaded MIL-100(Fe), initial weight loss was also observed at 100°C, indicating water loss and the removal of other organic solvents from the framework. An additional degradation was observed around 200°C, which corresponds to the presence of syringic acid in the framework. Lastly, the degradation at 450°C suggests the decomposition of MIL-100(Fe) and the reduction of iron. This findings conforms with the earlier study of Elharony and co-workers (2021) [59].

3.6. Surface Morphology and Particle Size Analysis

Micropictographs of the samples were taken using a scanning electron microscope at 15 kV and 20,000X magnification, with results presented in **Figure 4E**. MIL-100(Fe) exhibits a triangular-based pyramid shape that enhances drug absorption by maximizing surface area for drug loading, thus potentially improving therapeutic efficacy. After impregnation of syringic acid at 12 and 24 hours, the surface morphology of the particle did not significantly change in congruence with the PXRD data. The mean particle size of MIL-100(Fe) was reported as 270.67 nm ± 2.60 nm but upon loading with syringic acid resulted in 272.03 nm ± 1.33 nm (12-hours post loading), 269.67 nm ± 3.07 nm (24-hours post loading), 268.30 nm ± 0.40 nm (36-hours post loading), and 176.97 nm ± 4.67 nm (48-hours post loading).

 doi:10.20944/preprints202507.1970.v1

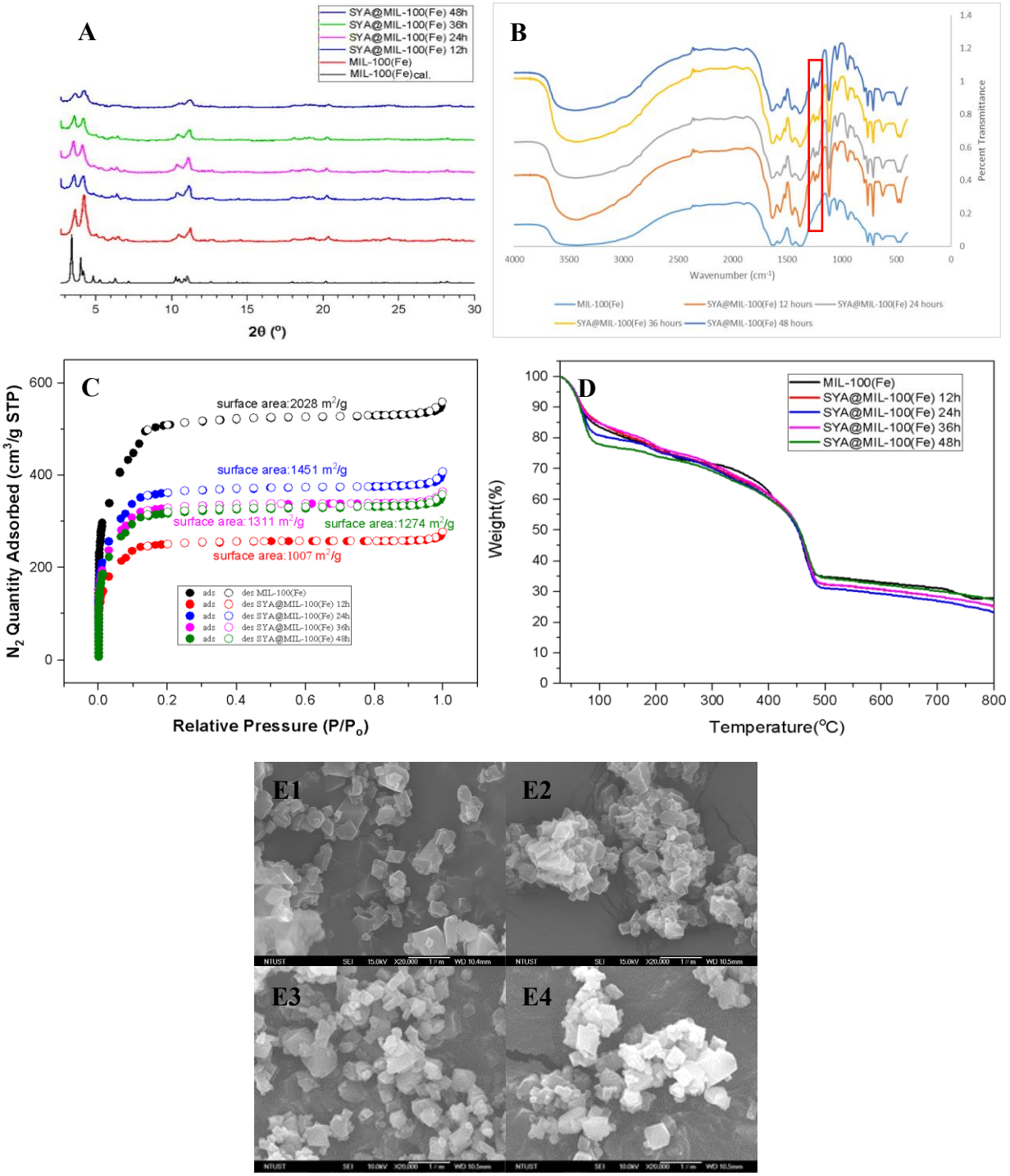

Figure 4. Characterization of MIL-100(Fe) and SYA@MIL-100(Fe) (A) XRD pattern, (B) infrared spectra, (C) nitrogen adsorption-desorption plot, (D) thermogram plot, and (E1) micro pictograph of MIL-100(Fe), (E2) SYA@MIL-100(Fe) at 12 hours, and (E3-4) SYA@MIL-100(Fe) at 24 hours taken at 10 kV and 20,000X magnification.

3.7. In Vitro Drug Release

The in vitro drug release of syringic acid was carried out using water, phosphate buffered saline (PBS) at pH 7.4 and pH 6.8, and 0.1 N hydrochloric acid as shown in **Figure 5**. After 30 hours, the cumulative release percentages of syringic acid were as follows: in water (94.67%), PBS pH 7.4 (117.55%), PBS pH 6.8 (110.93%), and 0.1N HCl (110.99%). Similarly, for SYA@MIL-100(Fe), the cumulative releases were 5.57% (water), 27.57% (PBS pH 7.4), 55.42% (PBS pH 6.8), and 25.80% (0.1

 doi:10.20944/preprints202507.1970.v1

N HCl). With these cumulative values of syringic acid released, it was deduced that there was a very slow release of syringic acid in the simulated release media. The data were plotted to determine the release kinetic profile at zero order kinetics, first order kinetics, Higuchi model, Korsmeyer–Peppas model, and Hixson-Crowell model.

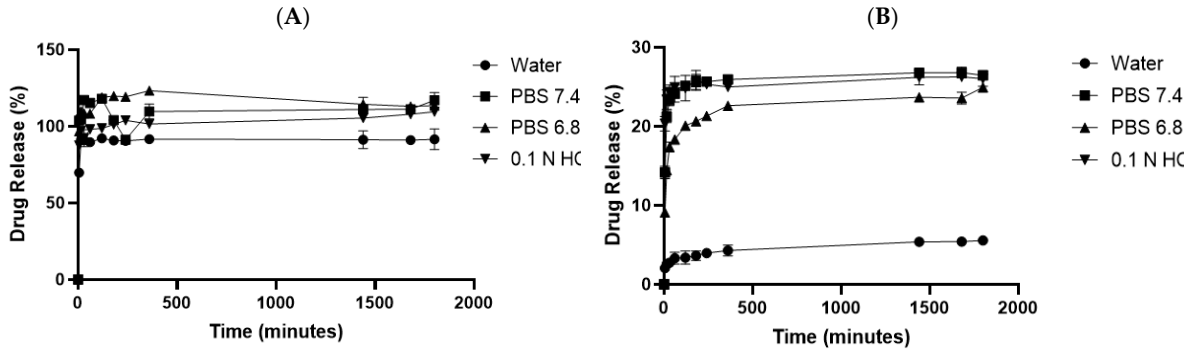

Figure 5. Cumulative drug release of (A) syringic acid and (B) SYA@MIL-100(Fe) in 4 different media. water, HCl—hydrochloric acid; PBS—phosphate buffered saline at pH 7.4 and 6.8. Data presented mean ± S.E.M.

3.8. Acute Oral Toxicity

Acute oral toxicity was performed to check the preliminary toxicity of syringic acid based on the Organization for Economic Cooperation and Development (OECD) 423 guidelines. The result indicates that the test samples at 2000 mg/kg were noted to be safe, as the test animals survived the 14 days of observation. Serological observation of the pre- and post-treatment resulted in a marked decrease in the test analysis of ALT, AST, BUN, and creatinine values, indicating that the samples were not toxic at the serological level. Histopathological analysis revealed distinct histopathological changes in liver and kidney structures across various rat models, with findings including mild to moderate hepatocellular degeneration and bile duct proliferation in the liver, and mild to moderate glomerular morphology and tubular degeneration in the kidneys. The cellular damage is determined not to be induced by the test sample due to the notable decrease in the serological analysis, and might be due to the sample preparation of the organs. With the OECD guidelines, the preparation was deemed to be classified as a "low toxicity" class.

3.9. Bioavailability

Bioavailability of syringic acid was determined by administering syringic acid alone and SYA@MIL-100(Fe). The pharmacokinetic parameters of syringic acid and SYA@MIL-100(Fe) were computed based on the noncompartment model and is shown in the Table. Figure 6 shows the mean plasma concentration-time curve of syringic acid in Sprague Dawley rats following both oral (100 mg/kg) and intraperitoneal (3 mg/kg) administration (data used in the graph is equated to 100 mg/kg). To have insights into the plasma concentration of syringic acid present in a certain amount of time, and to show systemic exposure to syringic acid, the area under the curve (AUC) was determined. Table 1 summarizes the pharmacokinetic parameters of syringic acid and SYA@MIL-100(Fe) obtained from the experimental data.

 doi:10.20944/preprints202507.1970.v1

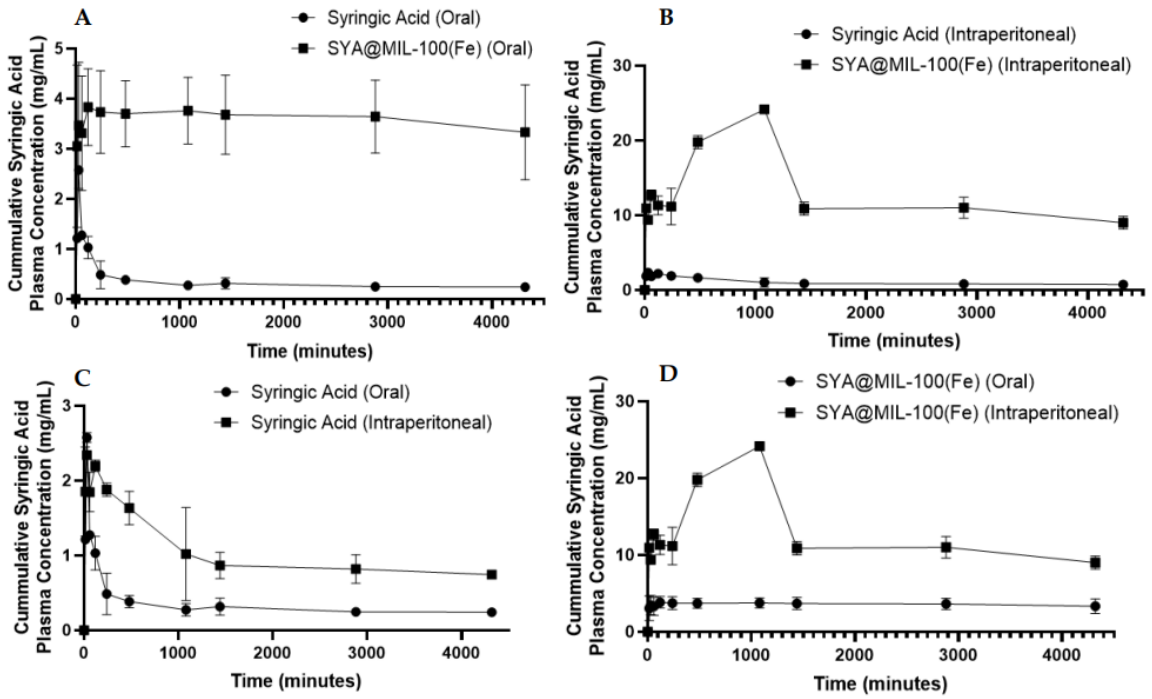

Figure 6. Area under the curve (AUC0–720) graph of (A) syringic acid (oral) and SYA@MIL-100(Fe) (oral), (B) syringic acid (intraperitoneal) and SYA@MIL-100(Fe) (intraperitoneal), (C) syringic acid (oral) and syringic acid (intraperitoneal), and (D) SYA@MIL-100(Fe) (oral) and SYA@MIL-100(Fe) (intraperitoneal) in Blood Samples. Data plotted as mean ± S.E.M. in time (minutes) and mean plasma concentration of syringic acid (mg/mL).

The area under the curve for the 0 time to 72 hours (AUC_{0-72}) of the syringic acid plasma concentration following oral administration of syringic acid and SYA@MIL-100(Fe) and intraperitoneal route of administration is shown in **Figure 6A-D**. The AUC_{0-72}) of administration was significantly higher in the SYA@MIL-100(Fe) (15606 ± 1936.03 mg min mL^{-1}) compared to syringic acid (1,419 ± 142.15 mg min mL^{-1}) alone when given through the oral route at a p-value of 0.02. In contrast, the AUC for the 0 time to infinity ($AUC_{0-\infty}$) showed no significant difference between the SYA@MIL-100(Fe) and syringic acid (131,269.97 ± 61,666.27 mg min mL^{-1} and 1,460 ± 143.84 mg min mL^{-1}, respectively) at a p-value of 0.103. The area under the curve for the 0 time to 72 hours (AUC_{0-72}) determined in the samples administered orally in the blood is significantly higher in the SYA@MIL-100(Fe) (15,606 ± 1936.03 mg min mL^{-1}) compared to syringic acid (1419 ± 142.15 mg min mL^{-1}) alone at a p-value of 0.02. In contrast, the AUC for the 0 time to infinity ($AUC_{0-\infty}$) showed no significant difference between the SYA@MIL-100(Fe) and Syringic acid (131,269.97 ± 61,666.27 mg min mL^{-1} and 1,460 ± 143.84 mg min mL^{-1}, respectively) at a p-value of 0.103. In congruence with the data of the AUC_{0-72}, significant differences were observed at the maximum concentration (C_{max}), and time to reach the maximum concentration (T_{max}) at p-values of 0.036 and 0.039, respectively. Between the two test groups, SYA@MIL-100(Fe) showed a significantly higher C_{max} (3.79 ± 0.43 mg mL^{-1}) and T_{max} (549.02 ± 159.41 min) compared to syringic acid alone (2.33 ± 0.19 mg mL^{-1} – C_{max} and 66.78 ± 7.56 min). The elimination half-life ($T_{1/2}$) between the two groups showed no significant difference at the p-value of 0.84 (SYA@MIL-100(Fe) – 24,392.75 ± 10,593.37 min vs Syringic Acid – 118.77 ± 30.76 min). The intraperitoneal route of administration showed a significant difference in all pharmacokinetic parameters p-values less than 0.05. The AUC_{0-72} of samples administered through the intraperitoneal route in the blood is significantly higher in the SYA@MIL-100(Fe) (56,022.33 ± 2,240.13 mg min mL^{-1}) compared to syringic acid (4368.33 ± 489.25 mg min mL^{-1}) alone when given through the oral route at a p-value less than 0.05. Likewise, the $AUC_{0-\infty}$ of SYA@MIL-100(Fe) (206,758.55 ± 31,210.34 mg min mL^{-1}) compared to syringic acid alone (5,400.84 ± 964.81 mg min mL^{-1}) at p-value of 0.03. SYA@MIL-100(Fe) showed significantly higher values for C_{max}, T_{max}, and $T_{1/2}$ (26.54 ± 0.55 mg mL^{-1}, 1,236.64 ±

 doi:10.20944/preprints202507.1970.v1

91.50 min, and 11,504.68 ± 2,306 min, respectively) compared to syringic acid alone (2.55 ± 0.04 mg mL^{-1}, 5.597 ± 2.11 min, and 999.64 ± 410 min, respectively).

The area under the curve for the 0 time to 72 hours (AUC0-72) of the syringic acid kidney concentration following oral administration of syringic acid and SYA@MIL-100(Fe) and intraperitoneal route of administration is shown in Figure 7A-D. The AUC0-72 determined in the samples administered orally in the kidney is significantly higher in the SYA@MIL-100(Fe) (130,698 ± 7713.74 µg min g-1) compared to syringic acid (77,103.33 ± 2,531.03 µg min g-1) alone at a p-value of 0.03. Likewise, the AUC for the 0 time to infinity (AUC0-∞) showed a significant difference between the SYA@MIL-100(Fe) and Syringic acid (144,112.76 ± 8494.44 µg min g-1 and 78,035.27 ± 2458.81 µg min g-1, respectively) at a p-value of 0.02. No significant difference was observed with maximum concentration (Cmax) between syringic acid (105.36 ± 9.79 µg g-1) and SYA@MIL-100(Fe) (89.27 ± 17.80 µg g-1) at a p-value of 0.473. In congruence with the AUC data, the time to reach the maximum concentration (Tmax) and elimination half-life (T1/2) were significantly higher in SYA@MIL-100(Fe) (97.30 ± 9.65 min, and 265.21 ± 22.01 min, respectively) compared to syringic acid alone (28.21 ± 0.33 min, and 37.56 ± 4.69 min, respectively) at p-values less than 0.05.

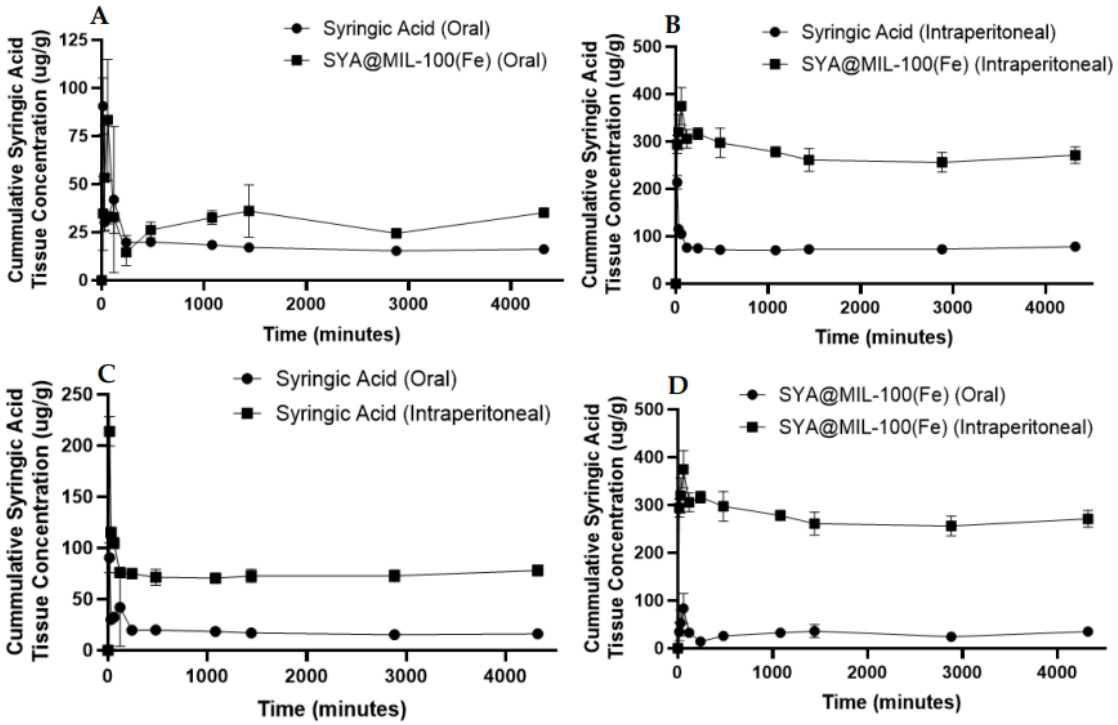

Figure 7. Area under the curve (AUC0–720) graph of (A) syringic acid (oral) and SYA@MIL-100(Fe) (oral), (B) syringic acid (intraperitoneal) and SYA@MIL-100(Fe) (intraperitoneal), (C) syringic acid (oral) and syringic acid (intraperitoneal), and (D) SYA@MIL-100(Fe) (oral) and SYA@MIL-100(Fe) (intraperitoneal) in Kidney Samples. Data plotted as mean ± S.E.M. in time (minutes) and mean tissue concentration of syringic acid (µg/g).

For the intraperitoneal route of administration using the kidney samples, significant differences were noted with AUC0-72, Cmax, and Tmax at p-values of less than 0.05. SYA@MIL-100(Fe) showed significantly higher pharmacokinetic parameters (1,169,999.33 ± 36,457.71 µg min g-1, 393.47 ± 14.44 µg g-1, and 118.08 ± 0.86 min, respectively) compared to syringic acid alone (321,104.67 ± 11,949.32 mg min mL-1, 218.21 ± 8,73 µg g-1, and 24.15 ± 0.96 min, respectively). No significant differences were noted on the AUC0-∞ and T1/2 for SYA@MIL-100(Fe) (2,971,634.10 ± 1,163,138.16 µg min g-1 and 2799.01 ± 1717.60 min, respectively) and syringic acid alone (808,296.10 ± 429,472.17 µg min g-1 and 4,805.81 ± 3271.08 min, respectively) at p-values of more than 0.05.

 doi:10.20944/preprints202507.1970.v1

The area under the curve for the 0 time to 72 hours (AUC_{0-72}) of the syringic acid liver concentration following oral administration of syringic acid and SYA@MIL-100(Fe) and intraperitoneal route of administration is shown in **Figure 8A-D**. The AUC_{0-72} determined in the samples administered orally in the liver is significantly higher in the syringic acid (32,000.33 ± 3544.16 μg min g^{-1}) compared to SYA@MIL-100 (Fe) (17,309.33 ± 1351.33 μg min g^{-1}) alone at a p-value of 0.018. Likewise, the AUC for the 0 time to infinity ($AUC_{0-\infty}$) showed a significant difference between the Syringic acid and SYA@MIL-100(Fe) (47,401.91 ± 8515.77 μg min g^{-1} and 22,623.03 ± 2085.19 μg min g^{-1}, respectively) at a p-value of 0.048. No significant difference was observed with maximum concentration (C_{max}) and elimination half-time ($T_{1/2}$) between syringic acid (16,2757 ± 3.54 μg g^{-1}, and 2,288.81 ± 812.6 min, respectively) and SYA@MIL-100(Fe) (11.42 ± 2.30 μg g^{-1}, and 913.33 ± 223.58 min, respectively) at a p-value of 0.31 and 0.18. In congruence, the maximum concentration (T_{max}) was significantly higher in Syringic acid (515.96 ± 4.44 min) compared to SYA@MIL-100(Fe) alone (385.57 ± 42.40 min) at p-value of 0.038.

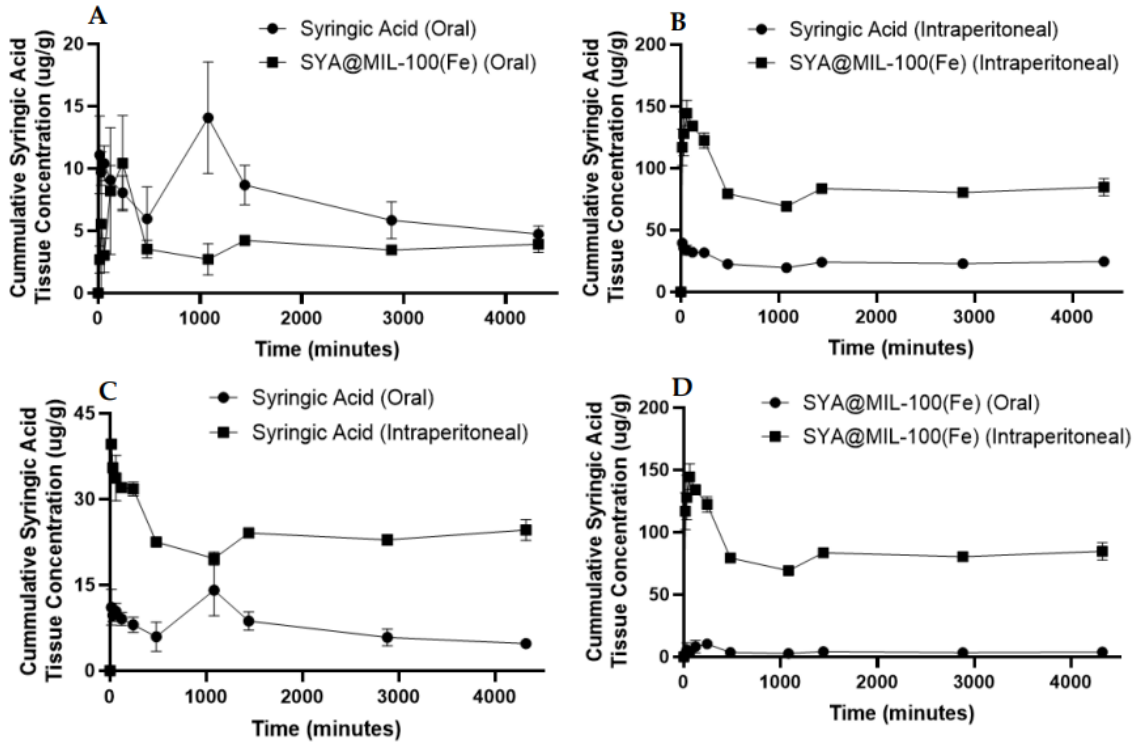

Figure 8. Area under the curve (AUC0–720) graph of (A) syringic acid (oral) and SYA@MIL-100(Fe) (oral), (B) syringic acid (intraperitoneal) and SYA@MIL-100(Fe) (intraperitoneal), (C) syringic acid (oral) and syringic acid (intraperitoneal), and (D) SYA@MIL-100(Fe) (oral) and SYA@MIL-100(Fe) (intraperitoneal) in Liver Samples. Data plotted as mean ± S.E.M. in time (minutes) and mean tissue concentration of syringic acid (μg/g).

For the intraperitoneal route of administration using the liver samples, significant differences were noted with AUC_{0-72}, $AUC_{0-\infty}$, C_{max}, and T_{max} at p-values of less than 0.001 and 0.003. SYA@MIL-100(Fe) showed significantly higher pharmacokinetic parameters (363,982.67 ± 5,429.14 μg min g^{-1}, 522, 988.13 ± 44,624.56 μg min g^{-1}, 150.26 ± 6.65 μg g^{-1}, and 111.01 ± 4.91 min, respectively) compared to syringic acid alone (102,784.67 ± 1,510.75 μg min g^{-1}, 166,522.15 ± 34,487.20 μg min g^{-1}, 40.13 ± 0.56 μg g^{-1}, and 24.70 ± 0.21 min, respectively). No significant difference was noted on $T_{1/2}$ for Syringic acid (1,852.40 ± 1,105.09 min) and SYA@MIL-100(Fe) (1309.25 ± 359.93 min) at p-value of 0.67.

Table 1. Summary of the pharmacokinetic parameters for oral and intraperitoneal route of syringic acid and SYA@MIL-100(Fe).

 doi:10.20944/preprints202507.1970.v1

Test Compound	Biological Sample	Route	AUC_{0-72}*	$AUC_{0-\infty}$*	C_{max}**	T_{max}***	$T_{1/2}$***
Syringic Acid	Blood	Oral	1,419 ± 142.15	1,460 ± 143.84	2.33 ± 0.19	66.78 ± 7.56‡	118.77 ± 30.76
		Intraperitoneal	4,368.33 ± 489.25‡	5,400.84 ± 964.81‡	2.55 ± 0.04‡	55.97 ± 2.11	999.64 ± 410‡
	Liver	Oral	32,000.33 ±3544.16‡	4,7401.91 ± 8,515.77‡	16.28 ±3.54	515.96 ± 4.44‡	2288.81 ± 812.66
		Intraperitoneal	102,784.67 ± 1510.75	166,522.15 ± 34,487.20	40.13 ± 0.56‡	24.70 ±0.21	1,852.40 ± 1,105.09
	Kidney	Oral	77,103.33 ± 2,531.03‡	78,035.27 ± 2,458.81‡	105.36 ± 9.79	28.21 ± 0.33‡	37.56 ± 4.69‡
		Intraperitoneal	321,104.67 ± 11949.32	808,296.73 ± 429,472.17	218.21 ± 8.73‡	24.15 ± 0.96	4,805.81 ± 3271.08
SYA@MIL-100(Fe)	Blood	Oral	15,606 ± 1,936.03	131,269.97 ± 61,666.27	3.79 ± 0.43	549.02 ± 159.41	24,392.75 ± 10,593.37
		Intraperitoneal	56,022.33 ± 2,240.13‡	206,758.55 ± 31,210.34‡	26.54 ± 0.55‡	1,236.64 ± 91.50‡	11,504.68 ± 2,306‡
	Liver	Oral	17,309.33 ± 1,351.33‡	22,623.03 ± 2,085.19‡	11.42 ±2.30	385.57 ± 42.44‡	913.33 ± 223.58
		Intraperitoneal	363,982.67 ± 5,429.14	522,988.13 ± 44,624.56	150.25 ±6.65‡	111.01 ± 4.91	1,309.25 ± 359.93
	Kidney	Oral	130,698 ± 7,713.74‡	144,112.76 ± 8494.44‡	89.27 ± 17.80	97.30 ± 9.65‡	265.21 ± 22.01‡
		Intraperitoneal	1,169,999.33 ± 36,457.71	2,971,634.10 ± 1,163,138.16	393.47 ± 14.44‡	118.08 ± 0.86	2,799.01 ± 1,717.60

* - unit of Area under the curve is mg min mL^{-1} (for blood sample) and ug min g^{-1} (for kidney and liver samples); ** - unit of C_{max} is mg mL^{-1}; *** - unit of T_{max} and $T_{1/2}$ is min; ‡ - significant differences at p value < 0.05.

4. Discussion

This is the first study utilizing Iron-based Metal-Organic frameworks as a drug carrier for syringic acid. MIL-100(Fe) (2) exhibited a sudden capture of syringic acid (1) in its framework, accounting for 64.42 ± 0.03% (~ 0.6442 mg of syringic acid per 1 mg of MIL-100(Fe)) during the 12-hour loading time, but decreased during the succeeding hours: 43.30 ± 0.17% (36 hours) > 39.12 ± 0.03% (24 hours) > 34.78 ± 0.04% (48 hours) at 1:2 ratio of MIL-100(Fe) and syringic acid. This phenomenon may be due to the potential framework collapse of the interaction of the nucleophilic center found in syringic acid [45,60], leading to ligand exchange or competition between the organic linker, trimesic acid, and syringic acid [61]. Decreased drug loading,12 hours loading (26.48% ± 0.03%) > 36 hours (26.38% ± 0.02%)> 48 hours (19.79% ± 0.02%) > 24 hours (19.28% ± 0.02%), was observed using the 1:1 ratio mainly due to the lower concentration of syringic acid available for impregnation. Researches confirmed that increasing the available drug or guest molecule can increase the drug loading into a carrier [62,63]. The remarkable drug loading of syringic acid with MIL-100(Fe) may be due to the physical properties of MIL-100(Fe), and the interaction of syringic acid with the framework. MIL-100(Fe) has been experimentally determined at 2,028 m^2/g (BET surface area), 0.950151 cm^3/g (pore volume), and 19.522 Å (pore size). This phenomenon has been supported by numerous researches [64–68]. Considering the particle diameter of syringic acid is 7.17 Å (as calculated, via semi-empirical optimization and energy minimization, using Chem3D Pro), this smaller particle diameter permits its own entry into the pore window of MIL-100(Fe), having a 19.522 Å pore size as computed using the nitrogen desorption-adsorption isotherm [69,70]. Lastly, the internal environment within the MIL-100(Fe) is considered amphiphilic, thus allowing the incorporation of both hydrophilic and hydrophobic drugs [45,71]. **Figure 9** shows the possible guest-interaction, which includes hydrogen bonding, π-π interaction, and iron complexation with phenolic rings [45,57,72,73]. Hydrogen can occur with the hydroxyl and carboxyl groups present in syringic acid, with the carboxyl group of trimesic acid. The π-π interaction can occur between syringic acid and the organic ligand. Finally, complexation of the iron moiety from MIL-100(Fe) and the nucleophilic oxygen in syringic acid occurs. This is evident by the change in color observed after exposing MIL-100(Fe) with syringic acid (pristine MIL-100(Fe) – color reddish brown) while SYA@MIL-100(Fe) – color dark to bluish reddish brown). Other possible mechanism is through electrostatic interaction[74]

 doi:10.20944/preprints202507.1970.v1

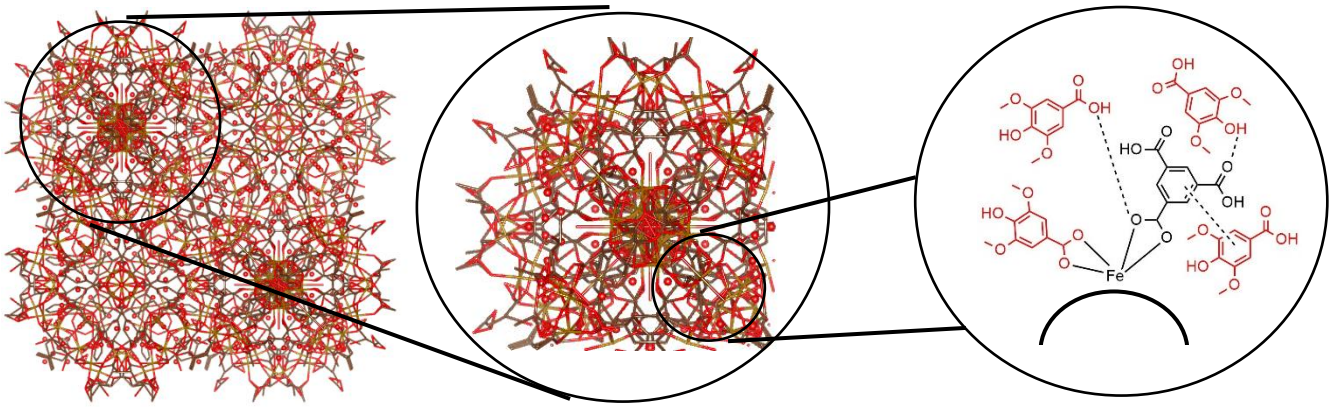

Figure 9. Predicted Binding of syringic acid into the MIL-100(Fe) framework using hydrogen bonding, π-π interaction, and iron complexation.

Other drugs that utilized MIL-100(Fe) as framework are the following oxaliplatin [75], curcumin [76], cyclophosphamide [77], chloroquine [78], doxycycline, tetracycline [39], cephalexin [79], lamivudine [80], and aceclofenac [81], noting that these drugs are bigger molecules compared to syringic acid. Thus, syringic acid having a smaller particle diameter can be entrapped inside the MIL-100(Fe). This findings is in congruence with the study of Santos and co-workers [45]. Compared to the other drug delivery systems reported for syringic acid, the entrapment efficiency of the preparation was lower compared to the work of Lin and co-workers (2020) utilizing mPEG-PLGA-PLL nanoparticles (EE of 92.69 ± 2.73%)[82], Sun and -coworker (2021) utilizing SMEDDS (EE of 98.04 ± 1.39%) [54], and Liu and co-workers (2019) utilizing TPGS Liposome (96.48 ± 0.76%)[12]. However, the studies did not report the use of percent drug loading, which measures the capacity of a given nanoparticle to carry or entrap a given drug. Shen and co-workers (2017) reported that varying the amount of drug during the drug loading affects the drug loading and entrapment efficiency[83]. The increase in the loading time also affects the amount of drug that can be incorporated into the framework up to a certain degree before the drug can alter the crystallinity of the framework [45].

The particle sizes of all MOFs were particularly within the range of nanoparticles (1-1000 nm) [84]. Another key consideration in the use of nanoparticles as drug delivery systems is their ability to enhance solubility, increase bioavailability, and, to a greater extent, pass the blood-brain barrier [84,85]. A smaller particle size is favorable for absorption due to a larger surface area [86]. In addition, MIL-100(Fe), ranging from 100 to 300 nm, is transported through the cell through clathrin or caveolin-mediated endocytosis [87]. The surface morphology of MIL-100(Fe) , in conformity with the previous studies, shows that octahedral nanoparticles are easily taken up by the cells through clathrin-mediated endocytosis [88]. Thus, MIL-100(Fe) is widely used as a drug carrier for different drugs [89].

The release of syringic acid in the four media resulted in 5.57% (ultrapure water), 27.57% (PBS pH 7.4), 55.42% (PBS pH 6.8), and 25.80% (0.1 N HCl) after 30 hours of release. These data indicate the SYA@MIL-100(Fe) preparation was pH dependent, as greater release in the PBS pH 6.8 media was noted. It can be noted that the release of syringic acid is notable on the PBS pH 7.4, pH 6.8, and 0.1 N HCl, but is less in distilled water. This is due to the presence of a nucleophilic moiety found on these media – the phosphate group in PBS media and chloride in diluted hydrochloric acid solution. The presence of these nucleophilic moieties destabilizes the structural integrity of MIL-100(Fe), which would lead to structural integrity and release of syringic acid [45,61,90,91]. Santos and co-workers cited that the presence of chloride ions with MIL-100(Fe) leads to protonation of the carboxylate group in the trimesic acid, resulting in incomplete reversible structural breakdown, while the presence of the phosphate group leads to competitive complexation with iron, thus displacing trimesic acid complexed with the iron moiety [45]. It can also be noteworthy that chloride and

 doi:10.20944/preprints202507.1970.v1

phosphate anions are present in the blood, thus providing a mechanism of gradual release inside the body.

The data were fitted to five mathematical models to determine the mechanism of syringic acid release. The models are noted as the Korsmeyer-Peppas model for water ($r^2 = 0.9788$) and 0.1N HCl ($r^2 = 0.9273$), the Higuchi Model for PBS pH 7.4 ($r^2 = 0.9162$), and the first-order release for PBS pH 6.8 ($r^2 = 0.9998$). Drug release studies of SYA@MIL-100(Fe) demonstrated that both water ($n = 0.1796$) and simulated gastric fluid ($n = 0.0824$) followed a **quasi-Fickian diffusion mechanism**, as indicated by their n-values below 0.45. This suggests that the release process was primarily governed by passive diffusion through the MOF's porous structure, with minimal influence from swelling or erosion. Comparable findings have been reported in other MOF-based systems, such as porous Zn-based MOF, where similarly low n-values reflected restricted molecular transport within rigid nanoporous matrices [92]. These results reinforce the potential of MIL-100(Fe) as a viable carrier for controlled, diffusion-based drug release under physiological conditions. The **Higuchi model** describes a drug release mechanism primarily governed by **diffusion through a porous matrix**. It assumes that the drug is uniformly dispersed within the carrier and that release occurs as the drug diffuses out over time, driven by a concentration gradient. This model is particularly applicable to non-swelling systems like metal-organic frameworks (MOFs), where structural stability and pore uniformity enable controlled diffusion-based release. Several MOFs have demonstrated Higuchi-type release behavior. For instance, the release of ketoprofen from Sr/PTA MOF [93], ibuprofen from UiO-66-NH_2 [94], and **doxorubicin from MOF [Cu_3(BTC)$_2$]**[95] showed sustained release consistent with diffusion through its mesoporous framework. The release kinetics of SYA@MIL-100(Fe) followed a first-order model, which is characterized by a concentration-dependent release rate. In this model, the rate of drug release decreases over time as the concentration of the encapsulated drug within the matrix decreases. This type of kinetic behavior is typical of systems where drug diffusion is the primary release mechanism and no significant burst release occurs. The sustained and controlled release profile provided by the MIL-100(Fe) matrix ensures gradual diffusion of syringic acid into the surrounding medium. Other metal-organic frameworks (MOFs) that have demonstrated first-order release kinetics include Folic acid from CD-MOF@SiO_2 nanocomposite[96] , and ibuprofen and captopril from Zr-MOF [68], both of which similarly showed prolonged, concentration-dependent drug release behavior, reinforcing the applicability of this model in MOF-based drug delivery platforms.

The acute oral toxicity result of the syringic acid and SYA@MIL-100(Fe) based on the OECD 423 guidelines at 2000 mg kg^{-1} aligns with the individual safety profile of syringic acid (Generally not considered as acute toxic agent based on the Safe work Australia – Code of Practice; no toxic effect at 14 days 1000 mg kg^{-1} daily administration for 14 days [97]) and MIL-100(Fe) (non-cytotoxic in human normal liver cells (HL-7702) and hepatocellular carcinoma (HepG2) [98]; non-toxic material [99]). It has been noted by Santos and co-workers that the collapse of the metal-organic framework with the presence of a more nucleophilic moiety can lead to framework destabilization and collapse, releasing the secondary building unit (SBU) complexed with the nucleophilic moiety, which is generally water-soluble [45].

The results of the serological data from the acute oral toxicity align with previously documented hepatoprotective properties of syringic acid, which include antioxidant activity, inhibition of lipid peroxidation, and modulation of inflammatory responses in the liver. However, the more pronounced reduction observed in our MIL-100(Fe) preparation suggests an added advantage: the sustained and targeted delivery enabled by the MIL-100(Fe) matrix likely enhanced tissue availability and therapeutic retention of syringic acid at hepatocellular sites. Compared to the free form—which is rapidly eliminated and limited by poor solubility—the MIL-100(Fe)-encapsulated syringic acid demonstrated slower systemic clearance and improved bioavailability, as supported by the pharmacokinetic data particularly significant higher AUC values of syringic acid in the liver compared to the blood (summarized in Table 1). This prolonged exposure may have allowed for more consistent antioxidant activity within liver tissue, thus minimizing cellular injury and enzyme

 doi:10.20944/preprints202507.1970.v1

leakage. The reduced AST and ALT levels in our experimental animals therefore not only reaffirm the intrinsic protective effect of syringic acid, as seen in CCl_4 [100]-, APAP [101]-induced models, thioacetamide-induced hepatic encephalopathy [102] and non-alcoholic fatty liver [103] , but also highlight the efficacy of MIL-100(Fe) as a delivery platform in enhancing the hepatoprotective potential of natural phenolic compounds. Overall, this supports the conclusion that the integration of syringic acid into the MIL-100(Fe) framework does not compromise its inherent safety and that the resulting formulation remains biocompatible under controlled conditions. While minimal liver changes, such as mild hepatocellular degeneration, were noted, there were no signs of severe toxicity or irreversible damage. These observations suggest that SYA@MIL-100(Fe) is generally safe for oral administration within the studied dose range. The results are consistent with existing literature on the parent compound. Syringic acid is widely recognized for its antioxidant and hepatoprotective properties.

Syringic acid is known to exhibit nephroprotective effects by lowering key kidney function markers such as BUN and creatinine, as demonstrated in diabetic nephropathy induced by streptozotocin [104,105], chronic hyperglycemia renal damage [106], renal oxidative stress and mitochondrial biogenesis [107]. This outcome supports the formulation's renal safety and aligns with the antioxidant properties of syringic acid.

The use of MIL-100(Fe) has been noted to increase the AUC_{0-72} values of syringic acid in both the oral (Syringic acid- 1,419 ± 142.15 mg min mL^{-1} vs SYA@MIL-100(Fe) - 15,606 ± 1,936.03 mg min mL^{-1}) and intraperitoneal routes (Syringic acid- 4,368.33 ± 489.25 mg min mL^{-1} vs SYA@MIL-100(Fe) - 56,022.33 ± 2,240.13 mg min mL^{-1}). Using the formula of the relative bioavailability and syringic acid as the reference, the relative bioavailability (F_{rel}) of SYA@MIL-100(Fe) over Syringic acid resulted in 10.997 (10.997 times greater). While the F_{rel} of the intraperitoneally administered SYA@MIL-100(Fe) over Syringic acid resulted in 12.82 (12.82 times greater). In comparison, the F_{rel} using the $AUC_{0-\infty}$ has increased to 89.91 and 38.28 (oral and intraperitoneal administration and comparison of SYA@MIL-100(Fe) over Syringic acid, respectively). These increases in the F_{rel} can be attributed to the use of the MIL-100(Fe) as a carrier. This is noted with a longer elimination half-life estimated using the non-compartment method (syringic acid - 118.77 ± 30.76 min (oral) and 999.64 ± 410 min (IP) versus SYA@MIL-100(Fe) - 24,392.75 ± 10,593.37 (oral) and 11,504.68 ± 2,306 min (IP)). This extended presence is consistent with the slow and sustained release characteristics of the MOF delivery system. As a result, less frequent dosing may be required to maintain therapeutic levels, reducing the potential for side effects associated with frequent administration. This lesser dosing frequency also contributes to improved patient adherence and compliance, which are critical factors in chronic or long-term therapies. Thus, the prolonged half-life not only supports the sustained-release nature of SYA@MIL-100(Fe) but also offers practical clinical advantages in terms of safety, convenience, and therapeutic consistency [108–110].

In congruence with the data of the *in vitro* drug release, the T_{max} for the SYA@MIL-100(Fe) (oral - 549.02 ± 159.41 min and IP- 1,236.64 ± 91.50 min) is longer compared to the syringic acid (oral - 66.78 ± 7.56 min and IP -55.97 ± 2.11 min) in both the oral and intraperitoneal route. The delayed T_{max} reflects the sustained release properties conferred by the MIL-100(Fe) structure, which acts as a reservoir that gradually releases the encapsulated compound into systemic circulation. This behavior is consistent with the intended function of MIL-100(Fe) as a controlled-release drug delivery system. Another key evidence in the use of MIL-100(Fe) is the C_{max} for both routes of SYA@MIL-100(Fe) (oral - 3.79 ± 0.43 mg mL^{-1} and IP - 26.54 ± 0.55 mg mL^{-1}) is greater compared to syringic acid alone (oral - 2.33 ± 0.19 mg mL^{-1} and IP - 2.55 ± 0.04 mg mL^{-1}). This suggests that the metal-organic framework effectively protects the active compound during gastrointestinal transit and promotes its gradual release and absorption across biological membranes, especially MIL-100(Fe) can activate the clathrin-mediated endocytosis. Interestingly, the use of the MIL-100(Fe) as a drug carrier provided a greater AUC_{0-72} of orally administered SYA@MIL-100(Fe) over intraperitoneally administered syringic acid, suggesting that the use of MIL-100(Fe) can promote the oral administration of drugs over the intraperitoneal route of administration. The same findings were noted in the study of Santos and co-workers with

 doi:10.20944/preprints202507.1970.v1

the increase in the systemic availability of magnolol using UiO-66(Zr) as a carrier [45]. The F_{rel} of the SYA@MIL-100(Fe) is greater than with the other research in the development of a drug delivery for syringic acid, such as TPGS/F127/F68 (2.3-fold) [111]; TPGS (2.8-fold) [12]; and SMEDDS (2.1-fold) [54].

The AUCs for both the experimental (0-72) and the calculated (0-∞) are far greater in SYA@MIL-100(Fe) compared to syringic acid alone, both for the oral and intraperitoneal route of administration in the liver and kidney samples. Greater AUCs are observed in the kidney samples compared to the liver samples, suggesting possible organ-specific accumulation of syringic acid, which may be attributed to active uptake mechanisms, or prolonged tissue retention [112]. Such accumulation of the drug in liver and kidney is consistent with existing literature on phenolic compounds, which are known to localize preferentially in metabolically active tissues, particularly the liver and kidney, due to their roles in detoxification, metabolism, and excretion processes [113–115]. Another potential reason for the increase in the concentration of syringic acid in the liver and kidney after use of MIL-100(Fe) as carrier is through the internalization of the hepatic phagocytes and renal phagocytes, and once inside the cells, the MIL-100(Fe) degrades due to the presence of nucleophilic moiety such as phosphate and others [18]

5. Conclusions

The study explores the potential of MIL-100(Fe) as a drug carrier for syringic acid. Experimental data show successful loading of syringic acid into the framework while still maintaining the structural integrity. Slow-release of syringic acid from MIL-100(Fe) is noted from the *in vitro* drug release study, supported by the T_{max} when administered orally and intraperitoneally to the Sprague Dawley rats. The increased AUC0–72, AUC0–∞, and C_{max} suggest that the systemic availability of syringic acid is increased, coupled with a prolonged elimination half-life. MIL-100(Fe) serves as a new avenue for a drug delivery system for syringic acid and potentially other low bioavailable drugs.

6. Patents

An ongoing patent application is being applied for this study.

Author Contributions: Conceptualization, JHS and CHL; methodology, JHS, HEL, MS, HJV, RZMW, SMV; formal analysis, JHS, CHL; investigation, X.X.; resources, JHS; data curation, JHS; writing—original draft preparation, JHS, MS, HJV; writing—review and editing, JHS, CHL, MS, HJV; visualization, RZMW; supervision, JHS, EAO, CHL, RZMW, SMV; project administration, JHS, EAO, CHL; funding acquisition, JHS, CHL. All authors have read and agreed to the published version of the manuscript.

Funding: This research was funded by the Department of Science and Technology – Philippines and the Ministry of Science and Technology -Taiwan through the MECO-TECO Joint Research Program.

Institutional Review Board Statement: The animal study protocol was approved by the Institutional Animal Care and Use Committee (IACUC) of the Department of Science and Technology – Industrial Technology Development Institute (Animal Research Permit AR-2024-0138, January 2024) for studies involving animals.

Informed Consent Statement: Not applicable.

Data Availability Statement: We encourage all authors of articles published in MDPI journals to share their research data. In this section, please provide details regarding where data supporting reported results can be found, including links to publicly archived datasets analyzed or generated during the study. Where no new data were created, or where data is unavailable due to privacy or ethical restrictions, a statement is still required. Suggested Data Availability Statements are available in section "MDPI Research Data Policies" at https://www.mdpi.com/ethics.

 doi:10.20944/preprints202507.1970.v1

Acknowledgments: Manila Economic and Cultural Office (MECO) and the Taipei Economic and Cultural Office (TECO) for providing an avenue for collaboration, DOST-ITDI Standards and Testing Division Laboratory for Animal Facility with key personnel: Julieta Brigoli, and Alvin V. Umali. Dr. Annabelle V. Briones, Director of DOST-ITDI, for the full support for this research. Pamela Berilyn So of Kaohsiung Medical University.

Conflicts of Interest: The authors declare no conflicts of interest.

Abbreviations

The following abbreviations are used in this manuscript:

MIL	Materials of Institut Lavoisier
MOF	Metal Organic Framework
AUC	Area under the Curve
C_{max}	Maximum Concentration
T_{max}	Time to reach maximum concentration
$T_{1/2}$	Half-life
SD	Sprague Dawley
SYA@MIL-100(Fe)	Syringic acid loaded MIL-100(Fe)

References

1. Molinari G. Natural Products in Drug Discovery: Present Status and Perspectives. In: Guzmán CA, Feuerstein GZ, editors. Pharm. Biotechnol., vol. 655, New York, NY: Springer New York; 2009, p. 13–27. https://doi.org/10.1007/978-1-4419-1132-2_2.
2. Gao S, Hu M. Bioavailability challenges associated with development of anti-cancer phenolics. Mini Rev Med Chem 2010;10:550–67. https://doi.org/10.2174/138955710791384081.
3. Kumar N, Goel N. Phenolic acids: Natural versatile molecules with promising therapeutic applications. Biotechnol Rep 2019;24:e00370. https://doi.org/10.1016/j.btre.2019.e00370.
4. Srinivasulu C, Ramgopal M, Ramanjaneyulu G, Anuradha CM, Suresh Kumar C. Syringic acid (SA) – A Review of Its Occurrence, Biosynthesis, Pharmacological and Industrial Importance. Biomed Pharmacother 2018;108:547–57. https://doi.org/10.1016/j.biopha.2018.09.069.
5. Hamaguchi T, Ono K, Murase A, Yamada M. Phenolic Compounds Prevent Alzheimer's Pathology through Different Effects on the Amyloid-β Aggregation Pathway. Am J Pathol 2009;175:2557–65. https://doi.org/10.2353/ajpath.2009.090417.
6. Estevinho L, Pereira AP, Moreira L, Dias LG, Pereira E. Antioxidant and antimicrobial effects of phenolic compounds extracts of Northeast Portugal honey. Food Chem Toxicol 2008;46:3774–9. https://doi.org/10.1016/j.fct.2008.09.062.
7. Chirinos R, Betalleluz-Pallardel I, Huamán A, Arbizu C, Pedreschi R, Campos D. HPLC-DAD characterisation of phenolic compounds from Andean oca (Oxalis tuberosa Mol.) tubers and their contribution to the antioxidant capacity. Food Chem 2009;113:1243–51. https://doi.org/10.1016/j.foodchem.2008.08.015.
8. Kumar N, Pruthi V. Potential applications of ferulic acid from natural sources. Biotechnol Rep 2014;4:86–93. https://doi.org/10.1016/j.btre.2014.09.002.
9. Pereira D, Valentão P, Pereira J, Andrade P. Phenolics: From Chemistry to Biology. Molecules 2009;14:2202–11. https://doi.org/10.3390/molecules14062202.
10. Pacheco-Palencia LA, Mertens-Talcott S, Talcott ST. Chemical Composition, Antioxidant Properties, and Thermal Stability of a Phytochemical Enriched Oil from Açai (*Euterpe oleracea* Mart.). J Agric Food Chem 2008;56:4631–6. https://doi.org/10.1021/jf800161u.
11. Pezzuto JM. Grapes and Human Health: A Perspective. J Agric Food Chem 2008;56:6777–84. https://doi.org/10.1021/jf800898p.
12. Liu Y, Sun C, Li W, Adu-Frimpong M, Wang Q, Yu J, et al. Preparation and Characterization of Syringic Acid–Loaded TPGS Liposome with Enhanced Oral Bioavailability and In Vivo Antioxidant Efficiency. AAPS PharmSciTech 2019;20:98. https://doi.org/10.1208/s12249-019-1290-6.

 doi:10.20944/preprints202507.1970.v1

13. Liu Y, Guo X, Lü Z, Xie W. Study on the pharmacokinetics and bioavailability of syringic acid in rabbits. Zhong Yao Cai Zhongyaocai J Chin Med Mater 2003;26:798–801.
14. Kumar S, Dilbaghi N, Rani R, Bhanjana G, Umar A. Novel Approaches for Enhancement of Drug Bioavailability. Rev Adv Sci Eng 2013;2:133–54. https://doi.org/10.1166/rase.2013.1038.
15. Gonçalves C, Pereira P, Gama M. Self-Assembled Hydrogel Nanoparticles for Drug Delivery Applications. Materials 2010;3:1420–60. https://doi.org/10.3390/ma3021420.
16. Sayed E, Haj-Ahmad R, Ruparelia K, Arshad MS, Chang M-W, Ahmad Z. Porous Inorganic Drug Delivery Systems—a Review. AAPS PharmSciTech 2017;18:1507–25. https://doi.org/10.1208/s12249-017-0740-2.
17. Liu S, Pan J, Ma Y, Qiu F, Niu X, Zhang T, et al. Three-in-one strategy for selective adsorption and effective separation of cis -diol containing luteolin from peanut shell coarse extract using PU/GO/BA-MOF composite. Chem Eng J 2016;306:655–66. https://doi.org/10.1016/j.cej.2016.07.111.
18. He S, Wu L, Li X, Sun H, Xiong T, Liu J, et al. Metal-organic frameworks for advanced drug delivery. Acta Pharm Sin B 2021;11:2362–95. https://doi.org/10.1016/j.apsb.2021.03.019.
19. Abánades Lázaro I, Abánades Lázaro S, Forgan RS. Enhancing anticancer cytotoxicity through bimodal drug delivery from ultrasmall Zr MOF nanoparticles. Chem Commun 2018;54:2792–5. https://doi.org/10.1039/C7CC09739E.
20. Bag PP, Wang D, Chen Z, Cao R. Outstanding drug loading capacity by water stable microporous MOF: a potential drug carrier. Chem Commun 2016;52:3669–72. https://doi.org/10.1039/C5CC09925K.
21. Cunha D, Ben Yahia M, Hall S, Miller SR, Chevreau H, Elkaïm E, et al. Rationale of Drug Encapsulation and Release from Biocompatible Porous Metal–Organic Frameworks. Chem Mater 2013;25:2767–76. https://doi.org/10.1021/cm400798p.
22. Gao H, Zhang Y, Chi B, Lin C, Tian F, Xu M, et al. Synthesis of 'dual-key-and-lock' drug carriers for imaging and improved drug release. Nanotechnology 2020;31:445102. https://doi.org/10.1088/1361-6528/aba65a.
23. He C, Lu K, Liu D, Lin W. Nanoscale Metal–Organic Frameworks for the Co-Delivery of Cisplatin and Pooled siRNAs to Enhance Therapeutic Efficacy in Drug-Resistant Ovarian Cancer Cells. J Am Chem Soc 2014;136:5181–4. https://doi.org/10.1021/ja4098862.
24. He Y, Zhang W, Guo T, Zhang G, Qin W, Zhang L, et al. Drug nanoclusters formed in confined nano-cages of CD-MOF: dramatic enhancement of solubility and bioavailability of azilsartan. Acta Pharm Sin B 2019;9:97–106. https://doi.org/10.1016/j.apsb.2018.09.003.
25. Horcajada P, Serre C, Maurin G, Ramsahye NA, Balas F, Vallet-Regí M, et al. Flexible Porous Metal-Organic Frameworks for a Controlled Drug Delivery. J Am Chem Soc 2008;130:6774–80. https://doi.org/10.1021/ja710973k.
26. Horcajada P, Chalati T, Serre C, Gillet B, Sebrie C, Baati T, et al. Porous metal–organic-framework nanoscale carriers as a potential platform for drug delivery and imaging. Nat Mater 2010;9:172–8. https://doi.org/10.1038/nmat2608.
27. Hu X, Wang C, Wang L, Liu Z, Wu L, Zhang G, et al. Nanoporous CD-MOF particles with uniform and inhalable size for pulmonary delivery of budesonide. Int J Pharm 2019;564:153–61. https://doi.org/10.1016/j.ijpharm.2019.04.030.
28. Leng X, Dong X, Wang W, Sai N, Yang C, You L, et al. Biocompatible Fe-Based Micropore Metal-Organic Frameworks as Sustained-Release Anticancer Drug Carriers. Molecules 2018;23:2490. https://doi.org/10.3390/molecules23102490.
29. Li X, Guo T, Lachmanski L, Manoli F, Menendez-Miranda M, Manet I, et al. Cyclodextrin-based metal-organic frameworks particles as efficient carriers for lansoprazole: Study of morphology and chemical composition of individual particles. Int J Pharm 2017;531:424–32. https://doi.org/10.1016/j.ijpharm.2017.05.056.
30. Li Z, Zhao S, Wang H, Peng Y, Tan Z, Tang B. Functional groups influence and mechanism research of UiO-66-type metal-organic frameworks for ketoprofen delivery. Colloids Surf B Biointerfaces 2019;178:1–7. https://doi.org/10.1016/j.colsurfb.2019.02.027.
31. Marcos-Almaraz MT, Gref R, Agostoni V, Kreuz C, Clayette P, Serre C, et al. Towards improved HIV-microbicide activity through the co-encapsulation of NRTI drugs in biocompatible metal organic framework nanocarriers. J Mater Chem B 2017;5:8563–9. https://doi.org/10.1039/C7TB01933E.

 doi:10.20944/preprints202507.1970.v1

32. Oh H, Li T, An J. Drug Release Properties of a Series of Adenine-Based Metal-Organic Frameworks. Chem - Eur J 2015;21:17010–5. https://doi.org/10.1002/chem.201501560.
33. Rezaei M, Abbasi A, Varshochian R, Dinarvand R, Jeddi-Tehrani M. NanoMIL-100(Fe) containing docetaxel for breast cancer therapy. Artif Cells Nanomedicine Biotechnol 2018;46:1390–401. https://doi.org/10.1080/21691401.2017.1369425.
34. Rojas S, Carmona FJ, Maldonado CR, Horcajada P, Hidalgo T, Serre C, et al. Nanoscaled Zinc Pyrazolate Metal–Organic Frameworks as Drug-Delivery Systems. Inorg Chem 2016;55:2650–63. https://doi.org/10.1021/acs.inorgchem.6b00045.
35. Simon MA, Anggraeni E, Soetaredjo FE, Santoso SP, Irawaty W, Thanh TC, et al. Hydrothermal Synthesize of HF-Free MIL-100(Fe) for Isoniazid-Drug Delivery. Sci Rep 2019;9:16907. https://doi.org/10.1038/s41598-019-53436-3.
36. Sun C-Y, Qin C, Wang C-G, Su Z-M, Wang S, Wang X-L, et al. Chiral Nanoporous Metal-Organic Frameworks with High Porosity as Materials for Drug Delivery. Adv Mater 2011;23:5629–32. https://doi.org/10.1002/adma.201102538.
37. Sun C-Y, Qin C, Wang X-L, Yang G-S, Shao K-Z, Lan Y-Q, et al. Zeolitic imidazolate framework-8 as efficient pH-sensitive drug delivery vehicle. Dalton Trans 2012;41:6906. https://doi.org/10.1039/c2dt30357d.
38. Sun K, Li L, Yu X, Liu L, Meng Q, Wang F, et al. Functionalization of mixed ligand metal-organic frameworks as the transport vehicles for drugs. J Colloid Interface Sci 2017;486:128–35. https://doi.org/10.1016/j.jcis.2016.09.068.
39. Taherzade S, Soleimannejad J, Tarlani A. Application of Metal-Organic Framework Nano-MIL-100(Fe) for Sustainable Release of Doxycycline and Tetracycline. Nanomaterials 2017;7:215. https://doi.org/10.3390/nano7080215.
40. Taylor-Pashow KML, Della Rocca J, Xie Z, Tran S, Lin W. Postsynthetic Modifications of Iron-Carboxylate Nanoscale Metal–Organic Frameworks for Imaging and Drug Delivery. J Am Chem Soc 2009;131:14261–3. https://doi.org/10.1021/ja906198y.
41. Zhang W, Guo T, Wang C, He Y, Zhang X, Li G, et al. MOF Capacitates Cyclodextrin to Mega-Load Mode for High-Efficient Delivery of Valsartan. Pharm Res 2019;36:117. https://doi.org/10.1007/s11095-019-2650-3.
42. Luo Y, Tan B, Liang X, Wang S, Gao X, Zhang Z, et al. Low-Temperature Rapid Synthesis and Performance of the MIL-100(Fe) Monolithic Adsorbent for Dehumidification. Ind Eng Chem Res 2020;59:7291–8. https://doi.org/10.1021/acs.iecr.9b06767.
43. Horcajada P, Surblé S, Serre C, Hong D-Y, Seo Y-K, Chang J-S, et al. Synthesis and catalytic properties of MIL-100(Fe), an iron(III) carboxylate with large pores. Chem Commun 2007:2820–2. https://doi.org/10.1039/B704325B.
44. Singco B, Liu L-H, Chen Y-T, Shih Y-H, Huang H-Y, Lin C-H. Approaches to drug delivery: Confinement of aspirin in MIL-100(Fe) and aspirin in the de novo synthesis of metal–organic frameworks. Microporous Mesoporous Mater 2016;223:254–60. https://doi.org/10.1016/j.micromeso.2015.08.017.
45. Santos JH, Quimque MTJ, Macabeo APG, Corpuz MJ-AT, Wang Y-M, Lu T-T, et al. Enhanced Oral Bioavailability of the Pharmacologically Active Lignin Magnolol via Zr-Based Metal Organic Framework Impregnation. Pharmaceutics 2020;12:437. https://doi.org/10.3390/pharmaceutics12050437.
46. Thommes M, Kaneko K, Neimark AV, Olivier JP, Rodriguez-Reinoso F, Rouquerol J, et al. Physisorption of gases, with special reference to the evaluation of surface area and pore size distribution (IUPAC Technical Report). Pure Appl Chem 2015;87:1051–69. https://doi.org/10.1515/pac-2014-1117.
47. Shahbazi S, Stratz SA, Auxier JD, Hanson DE, Marsh ML, Hall HL. Characterization and thermogravimetric analysis of lanthanide hexafluoroacetylacetone chelates. J Radioanal Nucl Chem 2017;311:617–26. https://doi.org/10.1007/s10967-016-5005-0.
48. Chao M-Y, Zhang W-H, Lang J-P. Co2 and Co3 Mixed Cluster Secondary Building Unit Approach toward a Three-Dimensional Metal-Organic Framework with Permanent Porosity. Molecules 2018;23:755. https://doi.org/10.3390/molecules23040755.
49. Bunaciu AA, Udriştioiu E gabriela, Aboul-Enein HY. X-Ray Diffraction: Instrumentation and Applications. Crit Rev Anal Chem 2015;45:289–99. https://doi.org/10.1080/10408347.2014.949616.

 doi:10.20944/preprints202507.1970.v1

50. So PB, Chen H-T, Lin C-H. De novo synthesis and particle size control of iron metal organic framework for diclofenac drug delivery. Microporous Mesoporous Mater 2020;309:110495. https://doi.org/10.1016/j.micromeso.2020.110495.
51. Danhier F, Magotteaux N, Ucakar B, Lecouturier N, Brewster M, Préat V. Novel self-assembling PEG-p-(CL-co-TMC) polymeric micelles as safe and effective delivery system for Paclitaxel. Eur J Pharm Biopharm 2009;73:230–8. https://doi.org/10.1016/j.ejpb.2009.06.015.
52. Baishya H. Application of Mathematical Models in Drug Release Kinetics of Carbidopa and Levodopa ER Tablets. J Dev Drugs 2017;06. https://doi.org/10.4172/2329-6631.1000171.
53. Ding P, Shen H, Wang J, Ju J. Improved oral bioavailability of magnolol by using a binary mixed micelle system. Artif Cells Nanomedicine Biotechnol 2018;46:668–74. https://doi.org/10.1080/21691401.2018.1468339.
54. Sun C, Li W, Zhang H, Adu-Frimpong M, Ma P, Zhu Y, et al. Improved Oral Bioavailability and Hypolipidemic Effect of Syringic Acid via a Self-microemulsifying Drug Delivery System. AAPS PharmSciTech 2021;22:45. https://doi.org/10.1208/s12249-020-01901-y.
55. Al Haydar M, Abid HR, Sunderland B, Wang S. Metal organic frameworks as a drug delivery system for flurbiprofen. Drug Des Devel Ther 2017;11:2685–95. https://doi.org/10.2147/DDDT.S145716.
56. Morris RE, Wheatley PS. Gas Storage in Nanoporous Materials. Angew Chem Int Ed 2008;47:4966–81. https://doi.org/10.1002/anie.200703934.
57. Wittmann T, Tschense CBL, Zappe L, Koschnick C, Siegel R, Stäglich R, et al. Selective host–guest interactions in metal–organic frameworks *via* multiple hydrogen bond donor–acceptor recognition sites. J Mater Chem A 2019;7:10379–88. https://doi.org/10.1039/C8TA12190G.
58. Zhu X, Gu J, Wang Y, Li B, Li Y, Zhao W, et al. Inherent anchorages in UiO-66 nanoparticles for efficient capture of alendronate and its mediated release. Chem Commun 2014;50:8779–82. https://doi.org/10.1039/C4CC02570A.
59. Elharony NE, El Sayed IET, Al-Sehemi AG, Al-Ghamdi AA, Abou-Elyazed AS. Facile Synthesis of Iron-Based MOFs MIL-100(Fe) as Heterogeneous Catalyst in Kabachnick Reaction. Catalysts 2021;11:1451. https://doi.org/10.3390/catal11121451.
60. Isaeva VI, Kustov LM. The application of metal-organic frameworks in catalysis (Review). Pet Chem 2010;50:167–80. https://doi.org/10.1134/S0965544110030011.
61. Li X, Lachmanski L, Safi S, Sene S, Serre C, Grenèche JM, et al. New insights into the degradation mechanism of metal-organic frameworks drug carriers. Sci Rep 2017;7:13142. https://doi.org/10.1038/s41598-017-13323-1.
62. Shano LB, Karthikeyan S, Kennedy LJ, Chinnathambi S, Pandian GN. MOFs for next-generation cancer therapeutics through a biophysical approach—a review. Front Bioeng Biotechnol 2024;12. https://doi.org/10.3389/fbioe.2024.1397804.
63. Wang Y, Zhang Y, Zhang X, Zhang Z, She J, Wu D, et al. High Drug-Loading Nanomedicines for Tumor Chemo–Photo Combination Therapy: Advances and Perspectives. Pharmaceutics 2022;14:1735. https://doi.org/10.3390/pharmaceutics14081735.
64. Bavnhøj CG, Knopp MM, Madsen CM, Löbmann K. The role interplay between mesoporous silica pore volume and surface area and their effect on drug loading capacity. Int J Pharm X 2019;1:100008. https://doi.org/10.1016/j.ijpx.2019.100008.
65. Raza A, Wu W. Metal-organic frameworks in oral drug delivery. Asian J Pharm Sci 2024;19:100951. https://doi.org/10.1016/j.ajps.2024.100951.
66. Cui R, Zhao P, Yan Y, Bao G, Damirin A, Liu Z. Outstanding Drug-Loading/Release Capacity of Hollow Fe-Metal–Organic Framework-Based Microcapsules: A Potential Multifunctional Drug-Delivery Platform. Inorg Chem 2021;60:1664–71. https://doi.org/10.1021/acs.inorgchem.0c03156.
67. Ahmadi M, Ayyoubzadeh SM, Ghorbani-Bidkorbeh F, Shahhosseini S, Dadashzadeh S, Asadian E, et al. An investigation of affecting factors on MOF characteristics for biomedical applications: A systematic review. Heliyon 2021;7:e06914. https://doi.org/10.1016/j.heliyon.2021.e06914.

 doi:10.20944/preprints202507.1970.v1

68. Cretu C, Nicola R, Marinescu S-A, Picioruș E-M, Suba M, Duda-Seiman C, et al. Performance of Zr-Based Metal–Organic Framework Materials as In Vitro Systems for the Oral Delivery of Captopril and Ibuprofen. Int J Mol Sci 2023;24:13887. https://doi.org/10.3390/ijms241813887.
69. Lee J, Wang L, Hou J. Emerging microporous materials as novel templates for quantum dots. Microstructures 2023. https://doi.org/10.20517/microstructures.2023.08.
70. Sun Y, Zheng L, Yang Y, Qian X, Fu T, Li X, et al. Metal–Organic Framework Nanocarriers for Drug Delivery in Biomedical Applications. Nano-Micro Lett 2020;12. https://doi.org/10.1007/s40820-020-00423-3.
71. Giménez-Marqués M, Hidalgo T, Serre C, Horcajada P. Nanostructured metal–organic frameworks and their bio-related applications. Coord Chem Rev 2016;307:342–60. https://doi.org/10.1016/j.ccr.2015.08.008.
72. Chobot V, Hadacek F. Iron and its complexation by phenolic cellular metabolites: From oxidative stress to chemical weapons. Plant Signal Behav 2010;5:4–8. https://doi.org/10.4161/psb.5.1.10197.
73. Singh K, Kumar A. Kinetics of complex formation of Fe(III) with syringic acid: Experimental and theoretical study. Food Chem 2018;265:96–100. https://doi.org/10.1016/j.foodchem.2018.05.071.
74. Quintero-Álvarez FG, Rojas-Mayorga CK, Mendoza-Castillo DI, Aguayo-Villarreal IA, Bonilla-Petriciolet A. Physicochemical Modeling of the Adsorption of Pharmaceuticals on MIL-100-Fe and MIL-101-Fe MOFs. Adsorpt Sci Technol 2022;2022:4482263. https://doi.org/10.1155/2022/4482263.
75. Sun B, Zheng X, Zhang X, Zhang H, Jiang Y. Oxaliplatin-Loaded Mil-100(Fe) for Chemotherapy–Ferroptosis Combined Therapy for Gastric Cancer. ACS Omega 2024;9:16676–86. https://doi.org/10.1021/acsomega.4c00658.
76. Parsa F, Setoodehkhah M, Atyabi SM. Design, fabrication and characterization of a magnetite-chitosan coated iron-based metal–organic framework (Fe_3O_4@chitosan/MIL-100(Fe)) for efficient curcumin delivery as a magnetic nanocarrier. RSC Adv 2025;15:18518–34. https://doi.org/10.1039/d5ra00162e.
77. Tohidi S, Aghaie-Khafri M. Cyclophosphamide Loading and Controlled Release in MIL-100(Fe) as anAnti-breast Cancer Carrier: In vivo In vitro Study. Curr Drug Deliv 2024;21:283–94. https://doi.org/10.2174/1567201820666230410120437.
78. Le BT, La DD, Nguyen PTH. Ultrasonic-Assisted Fabrication of MIL-100(Fe) Metal–Organic Frameworks as a Carrier for the Controlled Delivery of the Chloroquine Drug. ACS Omega 2023;8:1262–70. https://doi.org/10.1021/acsomega.2c06676.
79. Lajevardi A, Hossaini Sadr M, Tavakkoli Yaraki M, Badiei A, Armaghan M. A pH-responsive and magnetic Fe_3O_4@silica@MIL-100(Fe)/β-CD nanocomposite as a drug nanocarrier: loading and release study of cephalexin. New J Chem 2018;42:9690–701. https://doi.org/10.1039/c8nj01375f.
80. Sucharitha P, Reddy R, Jahnavi I, Prakruthi H, Sruthi T, Gowd MRGB, et al. Design of Lamivudine Loaded Metal Organic Frameworks MIL 100 (Fe) by Microwave Assisted Chemistry. Indian J Pharm Educ Res 2024;58:s1083–92. https://doi.org/10.5530/ijper.58.3s.108.
81. Al Haydar M, Abid HR, Sunderland B, Wang S. Multimetal organic frameworks as drug carriers: aceclofenac as a drug candidate. Drug Des Devel Ther 2018;Volume 13:23–35. https://doi.org/10.2147/dddt.s182983.
82. Lin Y, Yu R, Yin G, Chen Z, Lin H. Syringic acid delivered via mPEG-PLGA-PLL nanoparticles enhances peripheral nerve regeneration effect. Nanomed 2020;15:1487–99. https://doi.org/10.2217/nnm-2020-0042.
83. Shen S, Wu Y, Liu Y, Wu D. High drug-loading nanomedicines: progress, current status, and prospects. Int J Nanomedicine 2017;Volume 12:4085–109. https://doi.org/10.2147/IJN.S132780.
84. Rizvi SAA, Saleh AM. Applications of nanoparticle systems in drug delivery technology. Saudi Pharm J 2018;26:64–70. https://doi.org/10.1016/j.jsps.2017.10.012.
85. Kohane DS. Microparticles and nanoparticles for drug delivery. Biotechnol Bioeng 2007;96:203–9. https://doi.org/10.1002/bit.21301.
86. Liu D, Pan H, He F, Wang X, Li J, Yang X, et al. Effect of particle size on oral absorption of carvedilol nanosuspensions: in vitro and in vivo evaluation. Int J Nanomedicine 2015:6425. https://doi.org/10.2147/IJN.S87143.
87. Zhu J, Liao L, Zhu L, Zhang P, Guo K, Kong J, et al. Size-dependent cellular uptake efficiency, mechanism, and cytotoxicity of silica nanoparticles toward HeLa cells. Talanta 2013;107:408–15. https://doi.org/10.1016/j.talanta.2013.01.037.

 doi:10.20944/preprints202507.1970.v1

88. Linnane E, Haddad S, Melle F, Mei Z, Fairen-Jimenez D. The uptake of metal–organic frameworks: a journey into the cell. Chem Soc Rev 2022;51:6065–86. https://doi.org/10.1039/D0CS01414A.
89. Quijia CR, Lima C, Silva C, Alves RC, Frem R, Chorilli M. Application of MIL-100(Fe) in drug delivery and biomedicine. J Drug Deliv Sci Technol 2021;61:102217. https://doi.org/10.1016/j.jddst.2020.102217.
90. Neuer AL, Herrmann IK, Gogos A. Biochemical transformations of inorganic nanomedicines in buffers, cell cultures and organisms. Nanoscale 2023;15:18139–55. https://doi.org/10.1039/d3nr03415a.
91. Pirzadeh K, Ghoreyshi AA, Rohani S, Rahimnejad M. Strong Influence of Amine Grafting on MIL-101 (Cr) Metal–Organic Framework with Exceptional CO_2/N_2 Selectivity. Ind Eng Chem Res 2020;59:366–78. https://doi.org/10.1021/acs.iecr.9b05779.
92. Marson Armando RA, Abuçafy MP, Graminha AE, Silva RSD, Frem RCG. Ru-90@bio-MOF-1: A ruthenium(II) metallodrug occluded in porous Zn-based MOF as a strategy to develop anticancer agents. J Solid State Chem 2021;297:122081. https://doi.org/10.1016/j.jssc.2021.122081.
93. Li Z, Peng Y, Xia X, Cao Z, Deng Y, Tang B. Sr/PTA Metal Organic Framework as A Drug Delivery System for Osteoarthritis Treatment. Sci Rep 2019;9:17570. https://doi.org/10.1038/s41598-019-54147-5.
94. Lu L, Ma M, Gao C, Li H, Li L, Dong F, et al. Metal Organic Framework@Polysilsesequioxane Core/Shell-Structured Nanoplatform for Drug Delivery. Pharmaceutics 2020;12:98. https://doi.org/10.3390/pharmaceutics12020098.
95. Gharehdaghi Z, Naghib SM, Rahimi R, Bakhshi A, Kefayat A, Shamaeizadeh A, et al. Highly improved pH-Responsive anticancer drug delivery and T2-Weighted MRI imaging by magnetic MOF CuBTC-based nano/microcomposite. Front Mol Biosci 2023;10:1071376. https://doi.org/10.3389/fmolb.2023.1071376.
96. Liu S, Xiong Y, Dong F. Cyclodextrin metal–organic framework@SiO_2 nanocomposites for poorly soluble drug loading and release. RSC Adv 2024;14:31868–76. https://doi.org/10.1039/d4ra04935g.
97. Mirza AC, Panchal SS. Safety evaluation of syringic acid: subacute oral toxicity studies in Wistar rats. Heliyon 2019;5:e02129. https://doi.org/10.1016/j.heliyon.2019.e02129.
98. Chen G, Leng X, Luo J, You L, Qu C, Dong X, et al. In Vitro Toxicity Study of a Porous Iron(III) Metal–Organic Framework. Molecules 2019;24:1211. https://doi.org/10.3390/molecules24071211.
99. Tariq T, Bibi S, Ahmad Shah SS, Wattoo MA, Salem MA, El-Haroun H, et al. MIL materials: Synthesis strategies, morphology control, and biomedical application: A critical review. J Drug Deliv Sci Technol 2025;104:106532. https://doi.org/10.1016/j.jddst.2024.106532.
100. Itoh A, Isoda K, Kondoh M, Kawase M, Watari A, Kobayashi M, et al. Hepatoprotective Effect of Syringic Acid and Vanillic Acid on CCl4-Induced Liver Injury. Biol Pharm Bull 2010;33:983–7. https://doi.org/10.1248/bpb.33.983.
101. Ramachandran V, Raja B. Protective Effects of Syringic Acid against Acetaminophen-Induced Hepatic Damage in Albino Rats. J Basic Clin Physiol Pharmacol 2010;21. https://doi.org/10.1515/JBCPP.2010.21.4.369.
102. Ferah Okkay I, Okkay U, Gundogdu OL, Bayram C, Mendil AS, Ertugrul MS, et al. Syringic acid protects against thioacetamide-induced hepatic encephalopathy: Behavioral, biochemical, and molecular evidence. Neurosci Lett 2022;769:136385. https://doi.org/10.1016/j.neulet.2021.136385.
103. Zhang S, Zheng S, Li Y, Yang J, Mao X, Liu T, et al. Protective effects of syringic acid in nonalcoholic fatty liver in rats through regulation of Nrf2/HO-1 signaling pathway. J Biochem Mol Toxicol 2024;38. https://doi.org/10.1002/jbt.23809.
104. Sherkhane B, Yerra VG, Sharma A, Kumar KA, Chayanika G, Kumar AV, et al. Nephroprotective potential of syringic acid in experimental diabetic nephropathy: Focus on oxidative stress and autophagy. Indian J Pharmacol 2023;55:34–42. https://doi.org/10.4103/ijp.ijp_671_22.
105. Zabad OM, Samra YA, Eissa LA. Syringic acid ameliorates experimental diabetic nephropathy in rats through its antiinflammatory, anti-oxidant and anti-fibrotic effects by suppressing Toll like receptor-4 pathway. Metabolism 2022;128:154966. https://doi.org/10.1016/j.metabol.2021.154966.
106. Mirza AC, Panchal SS, Allam AA, Othman SI, Satia M, Mandhane SN. Syringic Acid Ameliorates Cardiac, Hepatic, Renal and Neuronal Damage Induced by Chronic Hyperglycaemia in Wistar Rats: A Behavioural, Biochemical and Histological Analysis. Molecules 2022;27:6722. https://doi.org/10.3390/molecules27196722.

 doi:10.20944/preprints202507.1970.v1

107. Rashedinia M, Khoshnoud MJ, Fahlyan BK, Hashemi S-S, Alimohammadi M, Sabahi Z. Syringic Acid: A Potential Natural Compound for the Management of Renal Oxidative Stress and Mitochondrial Biogenesis in Diabetic Rats. Curr Drug Discov Technol 2021;18:405–13. https://doi.org/10.2174/1570163817666200211101228.
108. Akram MU, Nesrullah M, Afaq S, Malik WMA, Ghafoor A, Ismail M, et al. An easy approach towards once a day sustained release dosage form using microporous Cu-MOFs as drug delivery vehicles. New J Chem 2024;48:11542–54. https://doi.org/10.1039/d3nj04569b.
109. Li L, Han S, Zhao S, Li X, Liu B, Liu Y. Chitosan modified metal-organic frameworks as a promising carrier for oral drug delivery. RSC Adv 2020;10:45130–8. https://doi.org/10.1039/d0ra08459j.
110. Kumar G, Kant A, Kumar M, Masram DT. Synthesis, characterizations and kinetic study of metal organic framework nanocomposite excipient used as extended release delivery vehicle for an antibiotic drug. Inorganica Chim Acta 2019;496:119036. https://doi.org/10.1016/j.ica.2019.119036.
111. Sun C, Li W, Ma P, Li Y, Zhu Y, Zhang H, et al. Development of TPGS/F127/F68 mixed polymeric micelles: Enhanced oral bioavailability and hepatoprotection of syringic acid against carbon tetrachloride-induced hepatotoxicity. Food Chem Toxicol 2020;137:111126. https://doi.org/10.1016/j.fct.2020.111126.
112. Coughlin JE, Pandey RK, Padmanabhan S, O'Loughlin KG, Marquis J, Green CE, et al. Metabolism, Pharmacokinetics, Tissue Distribution, and Stability Studies of the Prodrug Analog of an Anti-Hepatitis B Virus Dinucleoside Phosphorothioate. Drug Metab Dispos 2012;40:970–81. https://doi.org/10.1124/dmd.111.044446.
113. Spizzirri UG, Aiello F, Carullo G, Facente A, Restuccia D. Nanotechnologies: An Innovative Tool to Release Natural Extracts with Antimicrobial Properties. Pharmaceutics 2021;13:230. https://doi.org/10.3390/pharmaceutics13020230.
114. Lu J-L, Zeng X-S, Zhou X, Yang J-L, Ren L-L, Long X-Y, et al. Molecular Basis Underlying Hepatobiliary and Renal Excretion of Phenolic Acids of Salvia miltiorrhiza Roots (Danshen). Front Pharmacol 2022;13. https://doi.org/10.3389/fphar.2022.911982.
115. Wu Y, Li L, Ming G, Ma X, Liang C, Li Y, et al. Measurement of Pharmacokinetics and Tissue Distribution of Four Compounds from Nauclea officinalis in Rat Plasma and Tissues through HPLC-MS/MS. J Anal Methods Chem 2022;2022:1–18. https://doi.org/10.1155/2022/5297603.